Information-theoretic analysis of energy disposal in heavy-ion transfer reactions

Y. Alhassid

Department of Theoretical Physics, The Hebrew University, Jerusalem, Israel

R. D. Levine

Department of Physical Chemistry and Institute for Advanced Studies, The Hebrew University, Jerusalem, Israel

J. S. Karp and S. G. Steadman

Laboratory for Nuclear Science and Physics Department, Massachusetts Institute of Technology, Cambridge, Massachusetts 02139

Heavy-ion transfer reactions to highly excited states are examined in terms of surprisal analysis—a constrained statistical approach motivated by information-theoretic considerations. The practical use of the procedure is discussed and illustrated by application to the available data from a variety of reactions. The experimentally measured energy spectra for multinucleon transfer are found to be well described by a distribution of maximal entropy subject to constraints. These constraints are shown to imply that the distribution of single nucleon occupation numbers in the heavy residual nucleus is fully relaxed but that the two-particle (and higher) correlation functions are not. For few-nucleon transfers the energy spectra contain a second, smaller, component which is more strongly damped. The dynamical origin of the constraints is discussed in terms of sum rules derived from models for the transfer process. A simple model for grazing collisions which includes the effects of tangential friction (with the same damping constant for all exit channels) provides a qualitative and a quantitative account of the variation of the optimal Q value with the number of transferred nucleons.

NUCLEAR REACTIONS Heavy ions, ^{232}Th(^{16}O,X), $X=^{17,16,15}$N, ^{15,14,13,12}C, ^{13,12,11}B, ^{10}Be, $E=105$ MeV. ^{96}Mo(^{14}N,X), $X=^{15}$O, ^{13}C, ^{10}B, ^{9}Be, ^{7}Li, $E=97$ MeV. ^{A}Mo(^{14}N,X), $X=^{13}$C, ^{12}B, $A=100$, 98,97,96,95,94,92, $E=97$ MeV. ^{53}Cr(^{14}N,X), $X=^{13}$C, ^{11}B, ^{9}Be, $E=90$ MeV. ^{232}Th(^{15}N,X), $X=^{14,12}$C, ^{13,11}B, ^{10}Be, ^{9}Li, $E=145$ MeV. ^{232}Th(^{22}Ne,X),$X=^{26}$Na, ^{19,18}O, ^{17}N, ^{16,15}C, $E=174$ MeV. ^{197}Au(^{16}O,X), $X=^{15}$N, ^{11}B, ^{9}Be, $E=218$ and 250 MeV. Ni(^{16}O,^{12}C)Zn, $E=96$ MeV. Energy and nucleon occupation numbers in the ejectiles. Models for optimal Q values. Tangential friction.

I. INTRODUCTION

Heavy-ion transfer reactions at energies above the Coulomb barrier have been studied in considerable detail.[1-6] For a large number of reactions, double-differential (angle-energy) cross sections for the different final arrangement channels have been determined. We consider a method for correlating and compacting such data that centers attention on the relevant dynamical variables which constrain the evolution of the system. The description of the temporal development of such dynamical variables as charge and mass transfer during heavy-ion collisions has indeed profited from an approach based on transport equations.[7] Such an approach confirms, however, the implications evident from the raw distributions: despite the large number of accessible final states the distributions are not statistical. There is definite specificity in the population of the phase space after the collision.

The large value of the Sommerfeld parameter η, ($\eta=D/2\lambda$, the distance of closest approach divided by twice the de Broglie wave length) allows an essentially classical description of the orbit during such collisions.[8] Simple models for the transfer processes can thereby be developed.[9-15] These identify constraints, often termed "matching conditions," which need to be satisfied if the transfer is to be efficient, and hence preclude any entirely statistical distribution of final states.

The large value of D/λ, the high density of final states, and the specificity of energy disposal are also characteristic of molecular collisions.[16] There a procedure, surprisal analysis, which allows the incorporation of dynamical constraints into an otherwise statistical theory has been developed.[17] In a companion paper[18] the formal development of this analysis is discussed with special reference to collision processes (such as will be discussed below), where there is only partial resolution of the final states. Elsewhere,[19] it was shown how such a procedure can be used to provide solutions of the time-dependent Schrödinger equation.

Here we discuss the explicit application to experimental data and provide a surprisal analysis of the energy disposal in a variety of heavy-ion induced transfer reactions to highly excited states in the residual nucleus. The remarkably accurate description[20] of the experimentally measured energy distributions in terms of a small number of constraints demonstrates the considerable effectiveness of the present approach. The systematic variation of the surprisal parameter(s) shows the further correlation that can be achieved.

Section II discusses the essential elements of surprisal analysis and the procedure of maximal entropy. Particular attention is given to the surprisal plot, its interpretation and its sensitivity to systematic trends in the data. The application to specific heavy-ion transfer reactions is made in Sec. III. The representation of high quality data[21] on a surprisal plot enabled us to discern the presence of damped multistep processes for channels adjacent to the incident one. The implications of the observed constraints for the distribution of excitation energy in the residual nucleus are discussed in Sec. IV. The dynamical origin of the constraints in terms of sum rules is considered in Sec. V. By making a simple assumption on the form of the energy dissipation it is found possible to offer a quantitative sum rule for the mean final excitation energy (or for the Q value), using only a single damping constant for all exit channels. The concluding remarks in Sec. VI include a speculation on the possible future directions.

II. SURPRISAL ANALYSIS

In a strictly statistical theory those final quantum states that are allowed by the conservation laws are equally probable. The probability of any group of final states is then proportional to the number of states which belong to the group. The experimental results need not, however, conform to a uniform population of the accessible phase space. To examine the deviance of the observed distribution from that expected on purely statistical grounds it proves advantageous to introduce the concept of the surprisal. Let P_γ^0 be the probability of the group of final states γ, determined as the fraction of accessible final states which belong to the group γ. For an observed probability P_γ the surprisal is $-\ln(P_\gamma/P_\gamma^0)$. The surprisal is, therefore, a local measure of deviance from a purely statistical distribution. It can be computed for each group of final states and equals zero only for those groups for which $P_\gamma = P_\gamma^0$.

In a companion paper[18] and elsewhere[19] the connection of the surprisal to dynamical theories is examined. Here we comment briefly on the information-theoretic origin of the surprisal. Consid-

er the following situation: Let there be N_0 equally probable alternatives. When a definite, particular alternative is selected one has received $\ln N_0$ units of information.[22] Say, however, that instead of a definite particular alternative, a group consisting of N alternatives is selected. The amount of information received is now lower than $\ln N_0$ and equals $\ln N_0 - \ln N$ (since $\ln N$ units of information will be provided by selecting a particular alternative from the group of N). This argument leads to the following generalization: Before the selection each alternative had the probability $P^0 = 1/N_0$. After the selection the probability has been changed to $P = 1/N$. Hence the information received when the probability of an event γ is changed from P_γ^0 to P_γ is[22] $\ln(P_\gamma/P_\gamma^0)$. For an entire distribution the amount of information provided is

$$DS[P|P^0] \equiv \sum_\gamma P_\gamma \ln(P_\gamma/P_\gamma^0) . \qquad (2.1)$$

Equation (2.1) provides an integral measure of the deviance of the actual from the prior probabilities.

The phenomenological application of the surprisal depends on the observation that it often has a simpler structure than the raw data. Figure 1 shows an application to the distribution of excitation energy in the

$$^{16}O + {}^{232}Th \rightarrow {}^{12}C + {}^{236}U$$
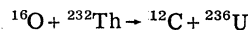
reaction.[21] The group γ is here the group of final quantum states when the translational energy is in the range E_f, $E_f + \Delta E_f$ [cf. (2.15) below]. The excitation energy is related to the final kinetic energy by energy balance ($E^* = E - E_f$). The prior distribution (discussed in detail in part C below) is monotonic and is a rapidly increasing function of the excitation energy. The observed distribution has an asymmetric bell shape. Yet the surprisal of the experimental results[21] is very nearly a linear function of the excitation energy. If one assumes that the surprisal is exactly linear [cf. Eq. (3.1) below] one obtains a distribution of excitation energies which is compared with the experimental histogram in the bottom panel of Fig. 1.

In a dynamical approach the cross section of any group γ of final states is given by $\sum'|T_{if}|^2\rho_f$ where the summation is restricted to those final states in the group γ and ρ_f is the translational density of states. Since the prior or statistical cross section is proportional to $\sum'\rho_f$ one can write

$$\sum'|T_{if}|^2\rho_f = \frac{\sum'|T_{if}|^2\rho_f}{\sum'\rho_f}\sum'\rho_f . \qquad (2.2)$$

The results in Fig. 1 can thus be regarded as a purely empirical finding: that the averaged $|T_{if}|^2$ element [the first factor on the right in (2.2)] has an exponential dependence on the excitation energy.
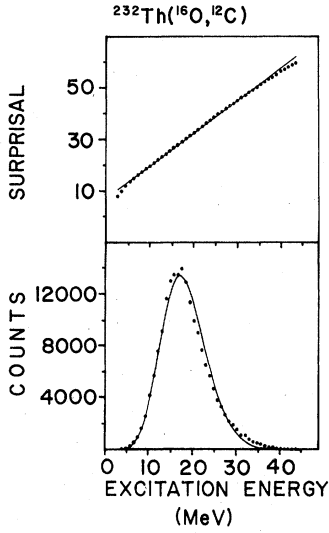
^{232}Th(^{16}O,^{12}C)

FIG. 1. The histogram of the distribution of final excitation energy in the ^{232}Th(^{16}O, ^{12}C)^{236}U channel (bottom panel) and its surprisal (dots, top panel) vs the excitation energy E^*. ($E^* = E - E_f$, where E is the total available energy: $E = E_i + Q_{gg}$. Q_{gg} is the ground state to ground state Q value.) Experimental results for $d^2\sigma/dE^*d\Omega$ at 70° and 105 MeV laboratory energy are from Ref. 21. The left ordinate shows the number of counts per channel. The surprisal of the experimental results (dots) is well approximated by a straight line. The distribution whose surprisal is exactly linear is shown as a continuous curve in the bottom panel and is in accord with the experimental histogram. The slope of the surprisal plot will be interpreted in Sec. IV as the inverse excitation temperature T_e^{-1} of the heavy residual nucleus.

In this fashion one has forged a link to parametrized versions[23] of distorted wave Born approximation (DWBA). However, it is clearly of interest to seek a more fundamental interpretation[18] of the functional form of the surprisal.

A. Procedure of maximal entropy

The entropy of a distribution of outcomes is given by[22]

$$S = -\sum_{f=1}^{N} P_f \ln P_f . \qquad (2.3)$$

It is non-negative and reaches its maximal value $(\ln N)$ for a uniform distribution when all outcomes are equally probable. It has the interpretation[22] of the amount of missing information when all we know are the probabilities. If the states f are grouped together such that there are g_γ states in the group γ and only the probabilities P_γ of the

different groups are given, we assign equal probability to all the states f within any particular group. The probability of any one quantum state within the group γ is thus given by

$$P_f = P_\gamma/g_\gamma \qquad (2.4)$$

and hence

$$S = -\sum_{f=1}^{N} (P_\gamma/g_\gamma) \ln(P_\gamma/g_\gamma)$$

$$= -\sum_{\gamma} P_\gamma \ln(P_\gamma/g_\gamma) .$$

The prior distribution is defined as the one of maximal entropy,

$$P_\gamma^0 = g_\gamma \Big/ \sum_{\gamma} g_\gamma = g_\gamma/N , \qquad (2.5)$$

so that

$$S = \ln N - \sum_{\gamma} P_\gamma \ln(P_\gamma/P_\gamma^0)$$

$$= S_{max} - DS[P|P^0] . \qquad (2.6)$$

Here $\ln N$ is the maximal value of the entropy. $DS[P|P^0]$ has been identified [cf. (2.1)] as the information provided when the distribution P_γ has been determined. It is seen here to be the difference between the maximal value of the entropy and its value for the distribution P_γ and is hence referred to as the entropy deficiency.[17] The inequality $\ln x \geq 1 - 1/x$ with equality if and only if $x = 1$ implies that DS is nonnegative and vanishes if and only if $P_\gamma = P_\gamma^0$ for all γ. Given any distribution P_γ one can compute $DS[P|P^0]$. The larger it is (the more information is conveyed by P_γ), the more, on the average, P_γ deviates from the prior distribution and the lower is its entropy.

The statistical distribution where all final quantum states (on the energy shell) are equally probable is the one of maximal entropy. Say the observed distribution is not statistical. One can still inquire whether it might be possible to characterize the observed distribution via a variational property of the entropy. In the companion paper[18] and elsewhere[24] it was argued that it makes sense to represent P as a distribution of maximal entropy subject to constraints. In other words, the distribution P deviates from the prior (or statistical) limit because it is subjected to constraints imposed by the dynamics of the collision. Apart from the need to accord with the value of the constraints the distribution P is as statistical as possible (i.e., of maximal entropy). In technical terms we can represent the value of the constraint A_r for the distribution P_γ by

$$\langle A_r \rangle = \sum_{\gamma} A_r(\gamma) P_\gamma . \qquad (2.7)$$

Here $A_r(\gamma)$ is the value of the constraint for the group γ. Since there are many groups γ, the value $\langle A_r \rangle$ of one constraint (or even a few values of different constraints) does not suffice to uniquely specify the values of the probabilities P_γ. The algorithm is thus: Among all the distributions P_γ which yield the same value of the constraint select P_γ^{ME} as the one of maximal entropy. Rather than seeking the constrained maximum of the entropy one can seek the unconstrained extremum of the Lagrangian

$$\mathcal{L} = -S + \lambda_0 \langle 1 \rangle + \sum_{r=1}^{n} \lambda_r \langle A_r \rangle . \tag{2.8}$$

Here $\langle 1 \rangle$ is the normalization condition

$$\langle 1 \rangle = \sum_\gamma P_\gamma , \tag{2.9}$$

and we have included n additional constraints in (2.8). The multipliers $\lambda_r, r = 0, 1, \ldots, n$ are Lagrange parameters. The resulting distribution of maximal entropy is[25]

$$P_\gamma^{ME} = P_\gamma^0 \exp\left[-\lambda_0 - \sum_{r=1}^{n} \lambda_r A_r(\gamma) \right] \tag{2.10}$$

and the values of the $n+1$ Lagrange parameters are determined by the values of the normalization $\langle 1 \rangle$ and of the other additional constraints. One can readily show that the result (2.10) is not just an extremum but yields the (unique[26, 27]) maximum of the entropy (subject to the constraints). In other words, all distributions P_γ which are consistent with the values of the constraints either are identical to (2.10) or have a lower entropy.

By construction, the distribution (2.10) is one of minimal information content. Any other distribution which is consistent with the constraints provides more information. This is the information-theoretic motivation for this prescription.[28] One should choose that distribution which is consistent with the constraints and is otherwise least informative. It represents the least biased (or maximally conservative) inference that can be made. The dynamical origin of the constraints has been discussed, in general, in the companion paper and is taken up again in Sec. IV.

B. Practical surprisal analysis

In part A we determined [cf. Eq. (2.10)] the distribution of maximal entropy subject to a given set of constraints. Here we consider the complementary problem: Given an experimental distribution P_γ, how do we choose a set of constraints that accounts well for the observation? Consider the Lagrangian $\mathcal{L}$, Eq. (2.8),

$$\mathcal{L} = \sum_\gamma P_\gamma \left[\ln(P_\gamma/P_\gamma^0) + \lambda_0 + \sum_{r=1}^{n} \lambda_r A_r(\gamma) \right] . \tag{2.11}$$

Here, however, the distribution P_γ is given and the minimum of $\mathcal{L}$ is to be determined by varying the Lagrange parameters.[27] Using (2.10), (2.11) can be written as

$$\mathcal{L} = \sum_\gamma P_\gamma \ln(P_\gamma/P_\gamma^{ME}) ,$$

or, in other words, each term in the square brackets in (2.11) is the difference between the predicted and the actual value of the surprisal. The inequality $\ln x \leq x - 1$ implies[27] that $\mathcal{L}$ is nonnegative and that a perfect fit obtains if and only if each term in (2.11) is identically zero. $\mathcal{L} = 0$ if and only if for each measured probability P_γ

$$-\ln(P_\gamma/P_\gamma^0) = \lambda_0 + \sum_{r=1}^{n} \lambda_r A_r(\gamma) . \tag{2.12}$$

Otherwise, the optimal fit is when $\mathcal{L}$ is minimal.[29] It should be noted, however, that the difference between the actual and predicted values of the surprisal contributes to $\mathcal{L}$ in proportion to P_γ. Hence the distribution of maximal entropy is not the one where the difference between the left- and right-hand sides in (2.12) is uniformly minimal. Rather, the high probability points are more heavily weighted in such a fit. For example, say only one constraint is imposed. The theoretical surprisal is then linear in $A(\gamma)$. In plotting $-\ln(P_\gamma/P_\gamma^0)$ vs $A(\gamma)$, one should not, therefore, aim for the best (in the sense of least squares) straight line. Rather, each point γ should be weighted as in (2.11). A computer program for such an analysis has been described[27] and is available upon request. Figure 2 is an example of the best linear surprisal fit to the energy spectrum in the ^{232}Th(^{16}O, ^{17}N)^{231}Pa re-

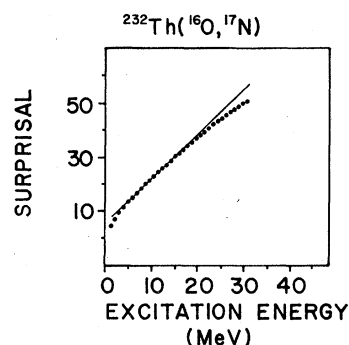FIG 2. Surprisal plot for the distribution of excitation energy in the ^{232}Th(^{16}O,^{17}N)^{231}Pa reaction. The surprisal of the experimental results (Ref. 21) (dots) is compared to the optimal linear surprisal [cf. Eq. (3.1) below]. A least square optimal straight line would lead to an even distribution of the deviances from the line.

action.[21] One could draw a line which appears to better represent the surprisal of the experimental data, $-\ln(P_\gamma/P_\gamma^0)$. But the line shown is the one which minimizes $\mathcal{L}$. In Sec. III we shall have more to say about the small but systematic deviations from a linear surprisal noted at high excitation energies for few-nucleon transfer processes.

In practice the Lagrange parameters are determined[27] by minimizing the (everywhere concave) function $\mathcal{L}(\lambda_1, \ldots, \lambda_n)$. One can, however, show[27] that this procedure is equivalent to the $n+1$ implicit equations

$$\sum_\gamma A_r(\gamma) P_\gamma = \sum_\gamma A_r(\gamma) P_\gamma^{ME}, \quad r = 0, 1, \ldots, n \qquad (2.13)$$

with $A_0(\gamma) = 1$. In other words, the values of the Lagrange parameters are chosen such that the mean values of the constraints are the same for the observed and the theoretical [cf. (2.10)] distributions.

The overall quality of the fit is given by the value of the Lagrangian $\mathcal{L}$ at the minimum. One can readily show that at that point

$$\min \mathcal{L} = \sum_\gamma P_\gamma \ln(P_\gamma/P_\gamma^{ME}), \qquad (2.14)$$

where P_γ is the experimental distribution while P_γ^{ME} is that distribution of maximal entropy which satisfies (2.13) [i.e., P_γ^{ME} has the functional form (2.10) with optimal values for the Lagrange parameters]. Hence (2.14) has the interpretation of the amount of information in the data not accounted for by the theory. Indeed, one can verify that

$$\min \mathcal{L} = \sum_\gamma P_\gamma \ln(P_\gamma/P_\gamma^{ME})$$
$$= DS[P|P^0] - DS[P^{ME}|P^0]. \qquad (2.14')$$

Because of the inevitable experimental scatter, it is not to be expected that a minimal $\mathcal{L} = 0$ will actually be reached. A fit which is within the experimental uncertainty has been obtained once the minimal value of $\mathcal{L}$ is about equal to the average square fractional error in the experimental distribution.[30]

C. The prior distribution for heavy-ion collisions

The prior distribution is computed on the basis of the fundamental assumption that all final quantum states that are allowed by the conservation laws are equally probable. Hence we take all the states allowed by energy conservation to be equally probable. The conservation of total angular momentum is imposed in an approximate but realistic fashion as is discussed below.

The distributions analyzed in this paper are those

of the final kinetic energy in heavy-ion induced reactions at incident energies above the Coulomb barrier. In this energy range the internal energy states of the excited heavy ejectile are either dense enough to be treated as a continuum or, for excitation energies above about 6 MeV, are actually in the continuum. Hence, the measured distribution is the fraction of collisions $P(E_f)\Delta E_f$ where the final kinetic energy is in the range E_f, $E_f + \Delta E_f$:

$$P(E_f) = (d^2\sigma/dE_f d\Omega)/(d\sigma/d\Omega). \qquad (2.15)$$

The prior distribution is then the (normalized) density of final states

$$P^0(E_f) = \rho(E_f) \bigg/ \int_0^E \rho(E_f) dE_f. \qquad (2.16)$$

Here $\rho(E_f)\Delta E_f$ is the number of final quantum states at a given total energy with the translational energy in the range E_f, $E_f + \Delta E_f$.

It should be noted that while the surprisal is defined as $-\ln[P(E_f)/P^0(E_f)]$, it is sufficient for most purposes to examine $-\ln[(d^2\sigma/dE_f d\Omega)/\rho(E_f)]$. The reason is that these two differ only in $\ln[(d\sigma/d\Omega)/\int dE_f \rho(E_f)]$ which is independent of E_f. Hence unless one needs the value of the normalization parameter λ_0 [cf. (2.10)] it is not necessary to normalize the energy spectrum.

The total energy is the sum of the translational and internal energies. Hence $\rho(E_f)$ is a product of the densities of the translational and internal states. A given internal energy can be partitioned between the two ejectiles. Hence the density of internal states is given as a convolution of the level densities of the two final nuclei.

In the region of higher internal energies one expects the nuclear level density to be roughly given by the degenerate Fermi-gas model,[31] which for a nucleus with rotational energy E_{rot} takes the form [Eq. (2.57) of Ref. 31]

$$\rho_I(E^*) \propto U^{-2} \exp[2(aU)^{1/2}]. \qquad (2.17)$$

Here U is the internal energy E^* adjusted for rotational energy and pairing effects:

$$U = E^* - E_{rot} - E_{pair}. \qquad (2.18)$$

To compute the rotational energy E_{rot} we have assumed a spheroidal rigid body moment of inertia and an angular momentum given by Rutherford orbit matching at the grazing angle. This estimate yields an E_{rot} which is quite small[20] compared to E^* (e.g., 0.57 MeV for the ^{12}C channel in the $^{16}O + ^{232}Th$ reaction shown in Fig. 1). Hence we allowed for conservation of total angular momentum in an approximate fashion by computing $\rho(U)$ using the mean value of the rotational energy. The pairing energy was estimated as[31] $E_{pair} = \delta \Delta_p$, where

$\delta = 0, 1$, or 2 for an odd-odd, even-odd, or even-even nucleus, respectively, and $\Delta_b = 12/A^{1/2}$ MeV where A is the mass number. The level density parameter in the Fermi gas was chosen to have the value[31] $a = A/8$. The implications of this choice are further discussed in Sec. IV. The excitation energy E^* is related to the Q value (final minus initial kinetic energy in the center-of-mass system) of the reaction $E^* = Q_{gg} - Q$, where Q_{gg} is the ground state to ground state Q value. For all the reactions analyzed the Q_{gg} values are from mass tables.[32] If a summation over a statistical distribution of final rotational states is carried out, (2.17) sums to

$$\rho_f(E^*) \propto (E^*)^{-5/4} \exp(2\sqrt{a E^*}) . \qquad (2.19)$$

In practice the exponential energy dependence overwhelms that of the preexponential factor.

For the reactions analyzed in this paper one final nucleus is always very much heavier than the other and hence has a far higher level density. Hence in convoluting the two level densities the heavier ejectile makes the dominant contribution. We have thus replaced the density of final internal states by the level density of the heavy ejectile. One can indeed argue analytically[33] that upon convoluting two level densities of the Fermi-gas type, the result is well approximated by the same functional form with a level density parameter which is the sum of the two. In other words, one expects the available excitation energy to be partitioned between the two products according to their mass. We have thus neglected the contribution to the energy due to the excitation of the lighter ejectile.

The density of translational states varies as[16,17] $E_f^{1/2}$. For all values of $E^* = E - E_f$ except those just below E, this variation is small compared to the rapid exponential variation of the density of internal states.

The strong variation of the prior distribution with energy has caused some concern among those who have not previously used surprisal analysis. It should therefore be explicitly stated that dividing $P(E_f)$ by the rapidly varying $P^0(E_f)$ fans out the experimental data and hence tends to amplify rather than to mask any systematic differences between the actual values of $-\ln(P_\gamma/P_\gamma^0)$ and the theoretical fit. Figure 2 which shows the surprisal for $^{232}\text{Th}(^{16}\text{O}, ^{17}\text{N})\,^{231}\text{Pa}$ channel is one illustration of this enhanced sensitivity. Deviations which are distinctly evident in a surprisal plot are just too small when a plot of $P(E_T)$ is examined. Similarly, Fig. 3 shows the sensitivity to the value of the level density parameter a, using the $^{232}\text{Th}(^{16}\text{O}, ^{12}\text{B})\,^{236}\text{Np}$ channel as an example.

III. RESULTS

Surprisal analysis of the existing data for heavy-ion transfer reactions to highly excited states has been carried out. The particular reactions[21,34-41] examined are listed in Table I. Among these, the 105 MeV $^{16}\text{O} + ^{232}\text{Th}$ data[21] will be considered in greater detail because of their considerably higher statistical accuracy. Only representative results for the other reactions will be reported. The conclusions, however, are based on an analysis of all the measured final channels in the reactions listed in Table I. The 96 MeV $^{16}\text{O} + \text{Ni}$ data[41] are obtained at a scattering angle well beyond the grazing angle and result from a deep-inelastic scattering process. They are included here to document the applicability of the analysis to such a process. All other data are obtained at or near the grazing angle. However, and as will be discussed in detail below, for channels adjacent to the incident one, the distributions can be resolved into a quasielastic and a smaller but more strongly damped component. The program used in the analysis has been discussed[27] and a user's copy with

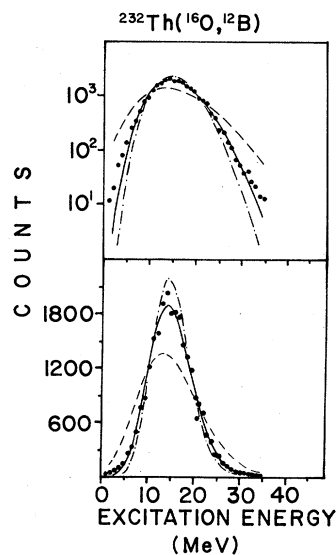$^{232}\text{Th}(^{16}\text{O}, ^{12}\text{B})$

FIG. 3. Histogram of the excitation energy distribution in the $^{232}\text{Th}(^{16}\text{O}, ^{12}\text{B})^{236}\text{Np}$ reaction (Ref. 21), on a linear (bottom) and logarithmic (top) scale. The continuous solid line is the best fit assuming an exactly linear surprisal [cf. Eq. (3.1)] and using $a = A/8$ for the level density parameter. The logarithmic plot serves to show the quality of the fit for the tail of the histogram. The width of the distribution (for a given most probable energy) is roughly proportional to $a^{-1/4}$ [cf. Eq. (3.12) below]. The dashed lines are fits using a higher ($a^{1/4} = 2.66$) and lower ($a^{1/4} = 1.76$) value of the level density parameter a ($a^{1/4} = 2.33$).

TABLE I. Heavy-ion induced reactions.[a]

Projectile	Target	E_{lab} (MeV)	E_i (MeV)	V_f^c (MeV)	θ	θ_{gr}	Exit channels measured	Ref.
^{16}O	^{232}Th	105	98.2	79.8	70	70	$^{17\text{-}15}$N, $^{15\text{-}12}$C, $^{13\text{-}11}$B, ^{10}Be	21
^{14}N	^{96}Mo	97	84.7	40.4	25	28	^{16,15}O, ^{13,12}C, $^{12\text{-}10}$B, ^{10,9,7}Be, ^{7,6}Li, ^{4}He	34
^{12}C	^{92}Mo	90	79.6	35.6	20	26	^{10}B, ^{10,9,7}Be, ^{7,6}Li	34
^{14}N	^{90}Zr	75	66.2	34.0	30	31	^{13,12}C, ^{11}B	34
^{14}N	^{A}Mo	97	85.1–84.2	40.0–40.8	25	28	^{13}C, ^{12}B	34
^{14}N	^{53}Cr	90	71.2	26.2	16	18	^{13,12}C, ^{11,10}B, ^{10,9,7}Be, ^{7,6}Li, ^{4}He	35
^{15}N	^{232}Th	145	136.2	70.2	40	38	$^{16\text{-}13}$C, $^{15\text{-}11}$B, $^{12\text{-}9}$Be, $^{11,9\text{-}7}$Li, ^{8,6}He	37
^{22}Ne	^{232}Th	174	158.9	96.6	40	42	$^{27\text{-}24}$Mg, $^{27\text{-}22}$Na, $^{25\text{-}20}$Ne, $^{23\text{-}18}$F, $^{22\text{-}15}$O, $^{20\text{-}14}$N, $^{18\text{-}12}$C, $^{14\text{-}10}$B, $^{12\text{-}9,7}$Be, $^{9\text{-}6}$Li	38
^{14}N	^{109}Ag	78	69.1	44.0	44	43	^{13,12}C	40
^{16}O	^{208}Pb	140	130.0	74.6	40	39	$^{17\text{-}13}$N, $^{15\text{-}11}$C, $^{13\text{-}10}$B, ^{10,9}Be	39
^{16}O	^{208}Pb	315	292.5	74.6	15	14	$^{15\text{-}13}$N, $^{14\text{-}11}$C, $^{12\text{-}10}$B, ^{10,9,7}Be, ^{7,6}Li	39
^{16}O	^{197}Au	218	201.6	72.8	25	21	^{15}N, ^{12}C, ^{11}B, ^{9}Be, ^{7,6}Li	39
^{16}O	^{197}Au	250	231.2	72.8	20	18	^{15}N, ^{12}C, ^{11}B, ^{9}Be, ^{7,6}Li	39
^{16}O	Ni	96	75.4	33.6	40	23	^{12}C	41

[a] The projectile, target, laboratory, and center-of-mass bombarding energies, entrance channel Coulomb barrier, (assuming $V_f^c = Z_1 Z_2 e^2 / [r_0(A_1^{1/3} + A_2^{1/3})]$ with $r_0 = 1.5$ fm and Z and A the charge and mass), laboratory scattering angle, laboratory grazing angle (assuming distance of closest approach on Rutherford orbit is $[r_0(A_1^{1/3} + A_2^{1/3}) + 1.5$ fm], with $r_0 = 1.45$ fm), arrangement channels measured and reference for the experimental results.

instructions is available upon request. For the purpose of the analysis those experimental results that are reported in the laboratory system have been transformed to the center-of-mass system. The transformation is based on the invariance of $d^3\sigma/d\vec{p}$ (where $\vec{p}$ is the momentum of the ejectile).

We proceed now to discuss each reaction listed in Table I. The section concludes with a summary of the results. Section IV considers the implication of the findings to the excitation energy disposal in the residual nucleus. A discussion of the dynamical origin of the constraints is provided in Sec. V.

A. ^{16}O + ^{232}Th at 105 MeV

These data obtained by the MIT group[21] at the Brookhaven tandem Van de Graaff facility span a total of 11 exit channels, namely $^{17\text{-}15}$N, $^{15\text{-}12}$C, $^{13\text{-}11}$B, and ^{10}Be ejectiles. The angular distributions are all bell shaped and centered at the grazing angle of 70°. The energy spectra are asymmetrically bell shaped. For most exit channels the counting statistics are excellent over a broad energy range (cf. bottom parts of Fig. 1), so that the statistical uncertainty in the data points is very small. Such data show to advantage the considerable sensitivity of the surprisal plot. Systematic effects that are barely evident in a linear

plot of the energy spectrum are quite evident in the surprisal (Fig. 2). The strongest exit channel is the $1p$ transfer (^{16}O, ^{15}N) reaction (which will be examined in detail in Fig. 6 below), followed in strength by the $2p$ transfer (^{16}O, ^{14}C) reaction. Even for one of the weaker channels (^{16}O, ^{17}N) the counting statistics suffice to take advantage of the sensitivity (cf. Fig. 2).

Figure 4 is a surprisal analysis of the (^{16}O, ^{17}N), (^{16}O, ^{14}C), and (^{16}O, ^{11}B) channels. The dashed straight lines in the top part show a fit to a linear form of the surprisal, i.e.,

$$-\ln[P^{ME}(E_f)/P^0(E_f)] = \lambda_0 + \lambda E^*. \quad (3.1)$$

Here E^* is the internal excitation energy

$$E^* = Q_{gg} - Q = Q_{gg} + E_i - E_f, \quad (3.2)$$

and the level density parameter a [cf. (2.17)] was chosen as $A/8$ MeV. The fit shown is a one parameter fit since λ_0 is a function of λ determined by the condition that the exit energy distribution $P(E_f)$ is normalized. We reiterate that the magnitude of λ is determined by the condition of maximal entropy [minimal information content, cf. (2.6)]. For the form (3.1) this means that $P^{ME}(E_f)$ and the experimental (normalized) energy spectrum $P(E_f)$

have the same mean energy [cf. (2.13)]:

$$\int E_f P^{\mathrm{ME}}(E_f)\,dE_f = \int E_f P(E_f)\,dE_f. \qquad (3.3)$$

Using (3.1) the condition (3.3) provides an implicit and nonlinear equation for λ:

$$\int E_f P^0(E_f)\exp(-\lambda E^*)\,dE_f \Big/ \int P^0(E_f)\exp(-\lambda E^*)\,dE_f$$

$$= \int E_f P(E_f)\,dE_f, \qquad (3.4)$$

where the right-hand side is available from the measured $d^2\sigma/dE_f\,d\Omega$ [cf. (2.15)]. An equivalent[27] and more practical route to the determination of λ is to minimize the Lagrangian $\mathcal{L}$ [cf. (2.11)], and this is the procedure recommended in practice, particularly if more than one constraint is employed.

The linear surprisal line with a slope λ implied by the condition (3.3) is shown in the top panels of Fig. 4. Our earlier comment [cf. the discussion of (2.11)] that the optimal surprisal line is not the least square line through the data points is evident.

The shown surprisal line clearly demonstrates the higher weight given to minimizing the deviance between the data $P(E_f)$ and the fit $P^{\mathrm{ME}}(E_f)$ at the more probable data points.

The linear surprisal provides a satisfactory but not spectacular account of the data. It correctly positions the peak of the distribution, and accounts for the asymmetry of the distribution (when plotted vs E^*), but fails to precisely determine the width. There is still enough statistical accuracy in the data to warrant the introduction of another constraint. Figure 4 also shows a fit to a two constraint form,

$$-\ln[P^{\mathrm{ME}}(E_f)/P^0(E_f)] = \lambda_0 + \lambda_1 E^* + \lambda_2 E^{*1/2}. \qquad (3.5)$$

The magnitudes of the Lagrange parameters are those implied by (3.3) and the corresponding condition on $E^{*1/2}$,

$$\int E^{*1/2} P^{\mathrm{ME}}(E_f)\,dE_f = \int E^{*1/2} P(E_f)\,dE_f. \qquad (3.6)$$

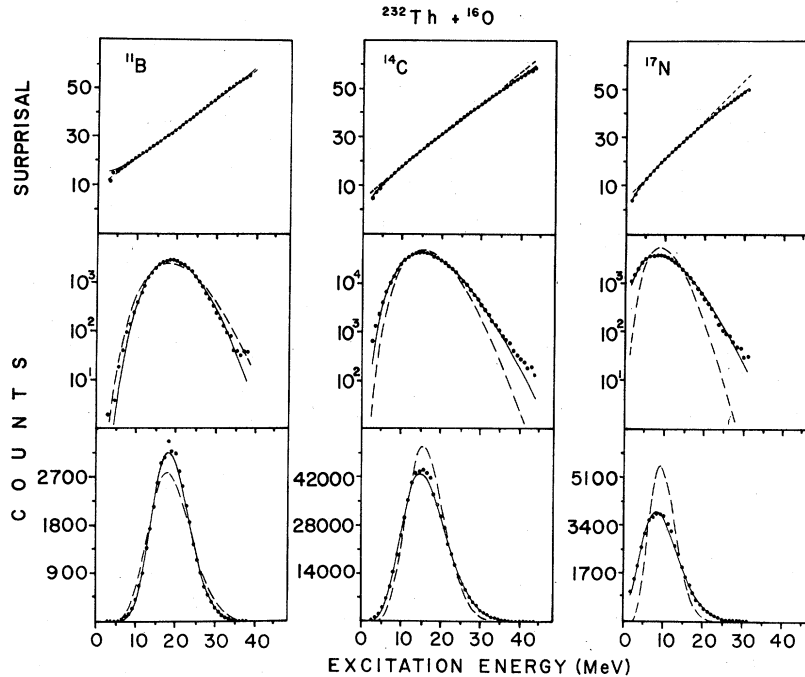As a practical point one should note that with the

²³²Th + ¹⁶O

FIG. 4. Surprisal analysis of the $(^{16}\mathrm{O},^{17}\mathrm{N})$, $(^{16}\mathrm{O},^{14}\mathrm{C})$, and $(^{16}\mathrm{O},^{11}\mathrm{B})$ channels showing the improved fit obtained by the introduction of the second constraint. Solid lines: a fit based on the two-constraint form, Eq. (3.5). Dashed lines: a fit based on the one-constraint form, Eq. (3.1). For $^{11}\mathrm{B}$, $\lambda_2 < 0$ so that the introduction of the second constraint serves to narrow down the distribution (or the surprisal vs E^* is concave). For $^{17}\mathrm{N}$ and $^{14}\mathrm{C}$, $\lambda_2 > 0$, the introduction of the secon constraint serves to widen the distribution (or the surprisal plot vs E^* is convex). The interpretation of the second constraint in terms of the exciton distribution in the heavy residual nucleus is discussed in Sec. IV. In particular, it is shown there that the slope of the linear surprisal fit (dashed line in the top panels) retains its interpretation as the (inverse) excitation temperature of the residual nucleus even when the experimental surprisal is not linear.

TABLE II. Analysis of the $^{16}O + ^{232}Th$ reaction at 105 MeV. [a]

Ejectile	$\langle E^*\rangle$ (MeV)	$a = A/8$ (MeV^{-1})	λ_1 (MeV^{-1})	λ_2 (MeV$^{-1/2}$)	T_e (MeV)	$(a^*/a)^{1/2}$	$DS[P|P^0]$	$DS[P|P^{ME}]$
^{17}N	9.5	28.88	0.79	5.4	0.60	0.50	23	2×10^{-3}
^{16}N	7.9	29.00	0.78	5.4	0.57	0.50	25	8×10^{-3}
^{15}N	6.6	29.13	1.0	5.3	0.49	0.51	15	3×10^{-3}
^{15}C	13.1	29.13	0.95	3.5	0.70	0.67	23	2×10^{-2}
^{14}C	16.4	29.25	0.90	3.4	0.75	0.68	24	2×10^{-3}
^{13}C	16.1	29.38	1.0	2.5	0.76	0.78	23	4×10^{-3}
^{12}C	17.9	29.50	1.1	1.6	0.78	0.86	22	8×10^{-3}
^{13}B	12.6	29.38	0.94	4.1	0.66	0.63	14	2×10^{-2}
^{12}B	15.1	29.50	1.3	0.61	0.74	0.94	18	7×10^{-3}
^{11}B	19.0	29.63	1.6	-3.4	0.81	1.3	16	4×10^{-3}
^{10}Be	24.5	29.75	2.7	-16	0.88	2.4	13	4×10^{-3}

[a] $\langle E^*\rangle$ is the measured centroid of the energy distribution. λ_1 and λ_2 are the Lagrange parameters for a two-constraint fit. $a^{*1/2} = a^{1/2} - \lambda_2/2$, where a is the level density parameter. For a good fit, $DS[P|P^{ME}] \ll DS[P|P^0]$, cf. Eq. (2.14'). The excitation temperature $T_e = 1/\lambda$, where λ is the Lagrange parameter for a one-constraint fit.

functional form (3.5), the equation (3.4) for λ_1 no longer holds [even though (3.3) remains valid]. Hence upon the introduction of a second constraint both λ_1 and λ_2 need be redetermined.

The fit using two constraints essentially exhausts the information content of the data [i.e., cf. (2.14), min$\mathcal{L} \simeq 0$]. The precise figures are given in Table II.

The choice of $E^{*1/2}$ as the second constraint was motivated by theoretical arguments examined in Sec. IV below and by the empirical finding that the surprisal plots for other exit channels (and other reactions) also sometimes show the same curvature at higher excitation energies which is seen in Fig. 4. We have, therefore, included the second constraint for all exit channels in the reaction, with the results shown in Fig. 5, and summarized in Table II. The sign of λ_2 reflects the curvature of the surprisal plot vs E^*. A positive value implies a downward trend as in the (^{16}O, ^{17}N) channel, Fig. 4, while a negative value corresponds to an upward trend as in the ^{10}Be or ^{11}B channels. In terms of the energy spectrum, if we keep the most probable value of E^* constant, increasing the width corresponds to increasing the value of λ_2 (cf. the discussion of Fig. 7 below).

In connection with the introduction of a second constraint, it is important to stress the following point: Because of the variational character of the maximum entropy formalism,[24] there is no possibility of adding "too many" constraints. If we include in the distribution P^{ME} a constraint which is not warranted, its (Lagrange) parameter will be found to be zero (or, in practice, owing to lack of absolute precision, very small). Such a constraint

is sometimes termed "noninformative," which reflects the theoretical relation[24]

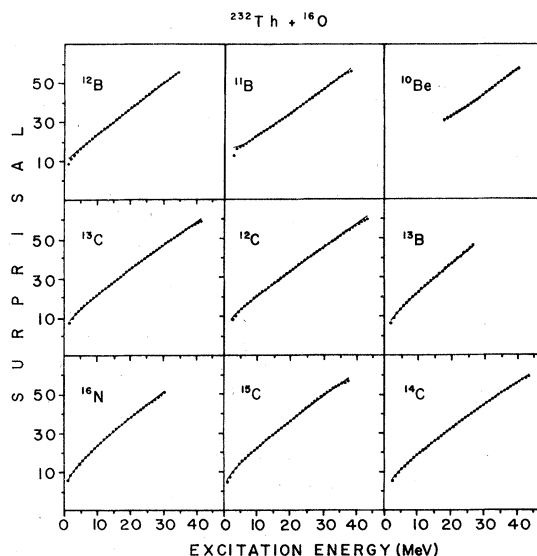$$\lambda_r = -\partial DS[P^{ME}|P^0]/\partial\langle A_r\rangle .\qquad(3.7)$$

FIG. 5. Surprisal plot of final arrangement channels in the $^{16}O + ^{232}Th$ reaction. The experimental results (Ref. 21) are compared with a two-constraint [Eq. (3.5)] fit (continuous line). For channels down to ^{12}B the surprisal is convex ($\lambda_2 > 0$) and below these it is concave ($\lambda_2 < 0$). The results for λ_1 and λ_2 are collected in Table II.

If $\lambda_r = 0$, then the mean value of the constraint does not change the information content of the distribution. If one is so inclined and the precision in the data warrants, one can include several constraints, and the surprisal analysis will weed out the noninformative ones.

A close examination of the $1p$ transfer channel ($^{16}O, ^{15}N$) in Fig. 6 shows a systematic deviance at the upper end of the excitation spectrum. Figure 6 shows that this high end is well fitted by a linear surprisal but with a reduced slope typical of the more relaxed channels such as ^{13}C. A simple interpretation of the surprisal plot for the ($^{16}O, ^{15}N$) channel is that the observed spectrum is composed of two components: a major peak with a low value of $\langle E^* \rangle$ which we interpret as a one-proton transfer reaction and a much smaller component with a higher value of $\langle E^* \rangle$ which is comparable to that of the ($^{16}O, ^{13}C$) channel. We suggest that the second component results from a three-nucleon transfer mechanism, as in the ($^{16}O, ^{13}C$) channel, except that in the ($^{16}O, ^{15}N$) channel two nucleons are transferred from projectile to target. Such bidirectional nucleon transfer has been previously discussed,[42] but the present results provide an experimental indication of this mechanism. Additional examples suggesting that one- or two-nucleon transfer processes can occur either via a direct, quasielastic or a bidirectional and more damped route will be discussed below for the other transfer reactions.

Assuming that the observed energy spectrum is the sum of two components, we have attempted a fit of the type

$$P^{ME}(E_f) = p P_q^{ME}(E_f) + (1-p) P_r^{ME}(E_f) , \qquad (3.8)$$

with the results shown in Fig. 6. The results for λ_1 and λ_2 in Table II refer to the dominant, quasielastic component of the spectrum. As a validation of this fit we have determined the surprisal parameter of the heavily damped, strongly relaxed $P_r^{ME}(E_f)$ component as follows: The quasielastic component P_q^{ME} is characterized by a low value of $\langle E^* \rangle$ and hence by a high value of λ_1. The major contribution to the tail (high E^*) end of the experimental spectrum is thus from the relaxed P_r^{ME} component. We have thus performed a surprisal analysis using only the high energy tail. (It is not necessary to have a normalized distribution to carry out a surprisal analysis. The Lagrange parameter λ_0 is a function of the other Lagrange parameters and need not be independently determined). The distribution $P_r^{ME}(E_f)$ which was determined in this fashion was then subtracted from the experimental $P(E_f)$ distribution. The dif-
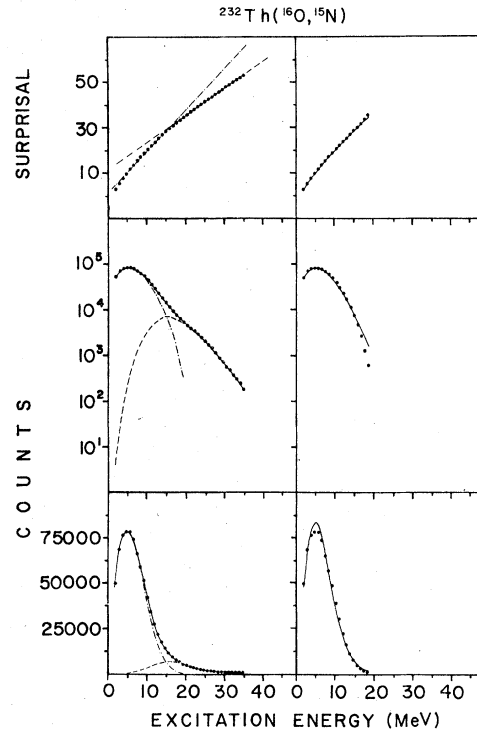

FIG. 6. The two component analysis [cf. Eq. (3.8)] of the ($^{16}O, ^{15}N$) channel. Left: the resolution of the experimental results (Ref. 21) (dots) into the quasielastic (major) and the nearly relaxed (minor) components. The solid line is the sum of the two. The excellent counting statistics are reflected in the accurate fit of the high energy tail as is evident in the logarithmic plot. Past $E^* > 20$ MeV the nearly relaxed process is the dominant contribution. Hence the slope of the surprisal plot past 20 MeV is the λ_1 parameter of the relaxed process. It is essentially the same slope as that of the ($^{16}O, ^{13}C$) channel. The surprisal of the quasielastic process (dot-dashed) has a higher slope. Right: surprisal analysis of the quasielastic component. (The distribution of energies for this component is obtained by subtracting the contribution of the more relaxed component, as is discussed in the text.)

ference was then subjected to surprisal analysis to determine the parameters of P_q^{ME}. Using either (3.8) or the peeling procedure gave the same results. A similar peeling procedure has also been employed in molecular collisions[43] to determine the presence of two components in the spectrum.

In conclusion, a fitted energy spectrum of the form

$$P^{ME}(E_f) = P^0(E_f)\exp(-\lambda_0 - \lambda_1 E^* - \lambda_2 E^{*1/2}) \qquad (3.9)$$

with a prior distribution computed using the degenerate Fermi-gas density of levels [cf. (2.17), $a = A/8$] is found to account for the data. A quick

estimate of the two parameters (λ_1 and λ_2) can be made by requiring that the functional form (3.9) accounts exactly for the value of the most probable excitation energy (E^*_{mp}) and for the full width at half maximum (FWHM) of the experimental spectrum. Such an estimate will not yield precise values but is sufficient for most purposes. Using the form (2.17) for the level density we can re-write (3.9) as

$$P^{ME}(E^*) \propto E^{*-2}\exp[2(aE^*)^{1/2} - \lambda_1 E^* - \lambda_2 E^{*1/2}]$$

$$= E^{*-2}\exp[2(a^*E^*)^{1/2} - \lambda_1 E^*]$$

with $a^* = (a^{1/2} - \lambda_2/2)^2$, and so we obtain for λ_1

$$\lambda_1 = (a^*/E^*_{mp})^{1/2} - 2/E^*_{mp}, \qquad (3.10)$$

where all quantities are in MeV units. The second term in (3.10) is quite small compared to the first (typically less than 0.2 MeV^{-1}). The two half maximum points occur at

$$(E^*_{1,2})^{1/2} \simeq (E^*_{mp})^{1/2} \pm [(E^*_{mp}/a^*)^{1/2}\ln 2]^{1/2} \qquad (3.11)$$

giving

$$\text{FWHM} = 3.33\, E^{3/4}_{mp}\, a^{*-1/4}. \qquad (3.12)$$

The spectrum is thus asymmetric even when $\lambda_2 = 0$ (so that $a^* = a$), and the dependence of the asymmetry on λ_2 is quite weak [since it is only $(a^*)^{1/4} = (a^{1/2} - \lambda_2/2)^{1/2}$ which governs the FWHM]. Nevertheless, for data with good statistics the values of λ_1 and λ_2 determined from (3.10) and (3.11) are quite reliable. Figure 7 compares the experimental values of $E^*_{1,2}$ to those predicted by (3.9). It also serves to show the asymmetry of the distribution.

Precise determinations of the three energies E^*_{mp} and $E^*_{1,2}$ suffice, therefore, to offer an over-

estimate of the two unknowns (λ_1 and λ_2) and hence of the entire spectrum.

Overall, we have demonstrated an excellent correspondence between the kinetic energy spectra at the grazing angle in the exit channels of the $^{16}O + {}^{232}Th$ reaction and the distributions determined by the procedure of maximal entropy subject to constraints. The significance and origin of these two constraints will be discussed below following the analysis of other reactions.

B. ^{12}C and ^{14}N on Mo, Zr, and Cr at energies above the Coulomb barrier

A large number of heavy-ion transfer reactions at energies up to three times the Coulomb barrier in the entrance channel have been studied[34-36] at the cyclotron facility of the Institute of Physical and Chemical Research, Saitama, Japan. The energy spectra show the same qualitative features as in the previous example except that the presence of a second component for few-nucleon transfer reactions is somewhat more manifest. All the reported[34,35] energy distributions for the reactions listed in Table I have been analyzed but only representative results will be shown. In examining the results one should note that since the cross sections are lower than in the $^{16}O + {}^{232}Th$ reaction the counting statistics are poorer. For many reactions (not listed in Table I) only the most probable Q values and $Q_{1,2}$ [cf. (3.11)] values were reported.[36] We have verified that these three values could usually be accounted for [using the estimates (3.10) and (3.11)] by two parameters, λ_1 and a^*.

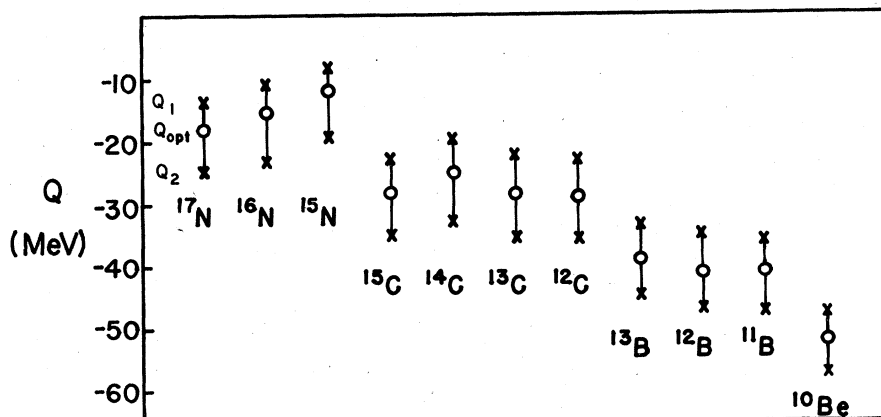Figures 8 and 9 show the results of surprisal analysis for the $^{14}N + {}^{96}Mo$ reaction[34] at a labora-

FIG. 7. The most probable (Q_{opt}) (dots) and half maximum ($Q_{1,2}$) (x) Q values for the different final channels of the $^{16}O + {}^{232}Th$ reaction (Ref. 21) at 105 MeV. The solid bar connects the $Q_{1,2}$ values determined via the distribution of maximal entropy subject to two constraints, Eq. (3.9).
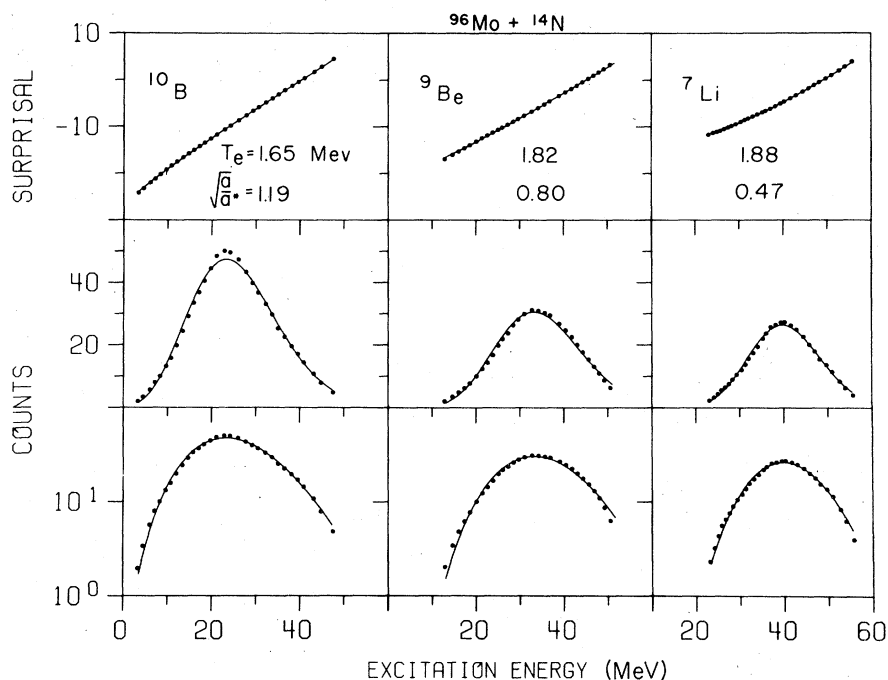
FIG. 8. Surprisal analysis of several multinucleon transfer processes in the ^{14}N$+^{96}$Mo reaction (Ref. 34) at 97 MeV, using the functional form (3.5). The parameters (cf. Sec. IV) given in the figure are $T_e = (a*/a)^{1/2}\lambda_1$ (in MeV), where $a* = (a^{1/2} - \lambda_2/2)^2$ and the ratio $(a/a*)^{1/2}$ [the ratio of the actual variance to that of a nucleus at thermal equilibrium at the temperature T_e, cf. Eq. (4.16)]. The logarithmic plot (bottom panels) of the experimental distribution serves to emphasize the asymmetry of the histogram.

tory energy of 97 MeV at 25°. The strongest exit channel is the $(1p, 1n)$ transfer (^{14}N, ^{12}C) reaction followed by the $(1p)$ transfer (^{14}N, ^{13}C) and then by (^{14}N, ^{11}B). All other channels are lower by at least an order of magnitude from the dominant process and the counts per energy channel are less than 100. The spectra at all channels are peaked at energies above the exit Coulomb barrier (the Coulomb repulsion of touching spheres, cf. Table I) and thus cannot be characterized as fully relaxed. Figure 8 shows the results for multinucleon transfers ^{96}Mo(^{14}N,X) for $X = ^{10}$B, ^{9}Be, ^{7}Li. The functional form (3.9), as used for the ^{16}O$+^{232}$Th analysis (cf. Fig. 5), accounts for the results. The parameters are listed in the figure. For few-nucleon transfers, Fig. 9, and, in particular, for the (^{14}N, ^{15}O) and the (^{14}N, ^{13}C) channels the need to allow for a second, more fully relaxed component is quite evident. The fit was performed using Eq. (3.8) and the parameters reported in the figure are for the quasielastic component. Similar results were obtained for the ^{12}C$+^{92}$Mo reaction[34] at 90 MeV, for the ^{14}N$+^{90}$Zr reaction at 75 MeV, and for the ^{14}N$+^{109}$Ag reaction (measured by the Orsay group[40]) at 78 MeV.

Figure 10 shows results for the same transfer process, ^{A}Mo(^{14}N, ^{12}B)$^{A+2}$Ru, for different Mo isotopes.[34] $A = 100$, 98, 97, 96, 95, 94, 92.

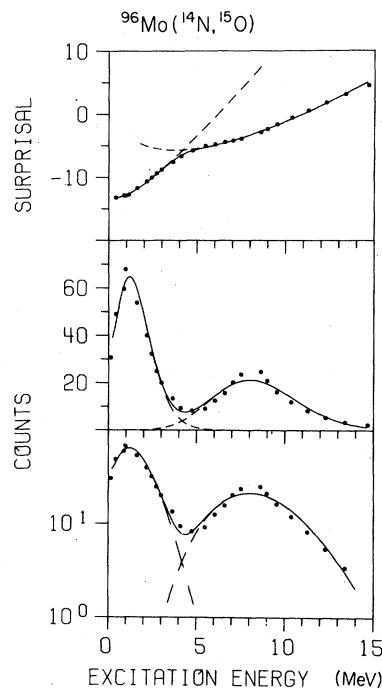FIG. 9. Surprisal analysis of the one-nucleon transfer (^{14}N, ^{15}O) channel in the ^{14}N$+^{96}$Mo reaction (Ref. 34) at 97 MeV. The fit is obtained using Eq. (3.8). A similar resolution was found possible for the other one-nucleon (^{14}N, ^{13}C) transfer process.

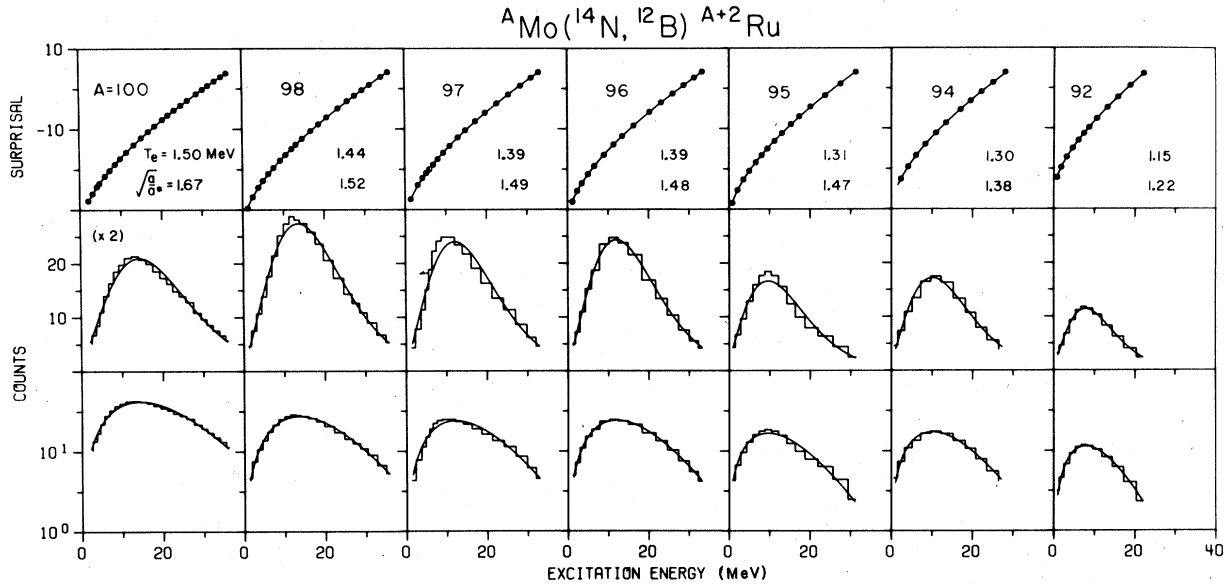$$^A\mathrm{Mo}(^{14}\mathrm{N},\,^{12}\mathrm{B})\,^{A+2}\mathrm{Ru}$$

FIG. 10. Surprisal analysis of the $^A\mathrm{Mo}(^{14}\mathrm{N},^{12}\mathrm{B})^{A+2}\mathrm{Ru}$ channels (Ref. 34) for A =100, 98, 97, 96, 95, 94, and 92 at 97 MeV. The two parameter fit, Eq. (3.5), is employed with the parameters T_e and $(a/a*)^{1/2}$ (cf. Fig. 8) shown in the drawing. For the one-nucleon transfer $^A\mathrm{Mo}(^{14}\mathrm{N},^{13}\mathrm{C})^{A+1}\mathrm{Tc}$ reactions there is evidence for a second, more strongly damped component.

E_L = 97 MeV at 25°. For a single nucleon transfer,[34] $^A\mathrm{Mo}(^{14}\mathrm{N},\,^{13}\mathrm{C})^{A+1}\mathrm{Tc}$, the analysis shows the presence of a second, strongly damped, component.

Energies up to three times higher than the Coulomb barrier have been studied[35] using targets of medium mass number. Figure 11 shows an analysis of the $^{14}\mathrm{N}+\,^{53}\mathrm{Cr}$ reaction at a laboratory energy of 90 MeV at 16°. The functional form (3.9) accounts well for the data. For one- or two-nucleon transfers we find clearcut evidence for a second and nearly fully relaxed component.
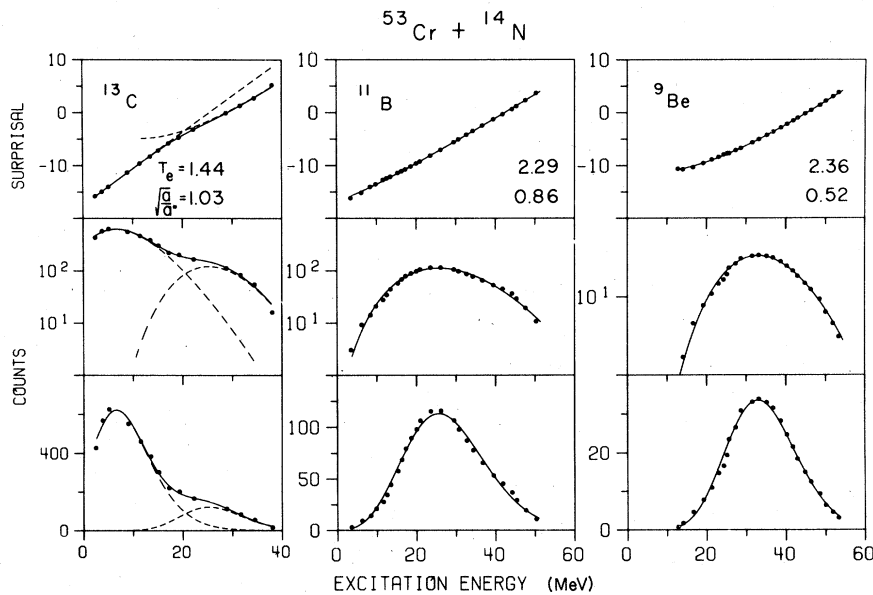
$$^{53}\mathrm{Cr} + \,^{14}\mathrm{N}$$

FIG. 11. Surprisal analysis of the $^{53}\mathrm{Cr}(^{14}\mathrm{N},^{13}\mathrm{C})^{54}\mathrm{Mn}$, $^{53}\mathrm{Cr}(^{14}\mathrm{N},^{11}\mathrm{B})^{56}\mathrm{Fe}$, and $^{53}\mathrm{Cr}(^{14}\mathrm{N},^{9}\mathrm{Be})^{58}\mathrm{Co}$ reactions (Ref. 35) at an incident energy (90 MeV) which is 2.5 times the Coulomb barrier in the entrance channel. For the one-nucleon transfer $(^{14}\mathrm{N},^{13}\mathrm{C})$ there is a second, nearly relaxed component. The parameters shown for this channel are for the quasi-elastic component.

C. ^{232}Th(^{15}N, X) at 145 MeV, ^{232}Th(^{22}Ne, X) at 174 MeV

Multinucleon transfer reactions have been extensively studied by the Dubna group.[2,37,38] An analysis of several channels in the ^{15}N + ^{232}Th collision at 40° is shown in Fig. 12. To within the error bars, the two-parameter fit of Eq. (3.9) accounts well for the results. At the higher energy ^{22}Ne + ^{232}Th collision, several exit channels show what appears as a second process at energies below the Coulomb barrier in the exit channel. Except for this feature (which is not present in most of the channels), the functional form (3.9) is, in general, Fig. 13, in accord with the data.

The systematic trends of the isotope production cross sections [1-3] were first discussed by the Dubna group.[2,37,38] It remains to be shown that the constraints identified in the present study suffice to account for these branching ratios.[44,45]

D. ^{208}Pb(^{16}O, X) and ^{197}Au(^{16}O, X)

The data obtained using the ^{16}O beam produced by the 88-inch cyclotron at the Lawrence Berkeley Laboratory is at a somewhat higher energy.[3,4,39,40] Figure 14 shows an analysis of two channels, ^{197}Au(^{16}O, ^{11}B)^{202}Pb and ^{197}Au(^{16}O, ^{9}Be)^{204}Bi, at the energies of 218 and 250 MeV at about 25° and 20°, respectively. We have not found it necessary to appeal to a fragmentation model,[3,4,39] and the two-body point of view adopted in this paper suffices to fit the results and to account for the asymmetry of the energy distribution. As in the other reactions, a one-nucleon transfer process, e.g., ^{197}Au(^{16}O, ^{15}N)^{198}Hg, does show the presence of a smaller and strongly damped contribution, Fig. 15.

E. Ni(^{16}O, ^{12}C)Zn at 96 MeV

The previous examples would not usually be described as deep-inelastic or as strongly damped collisions. Their angular distributions were peaked about the grazing angle and the optimal Q values of the energy spectrum were not fully relaxed. Here we consider an example where the angular distribution is forward peaked[41] and analyze the energy spectrum at an angle of 40° (lab), well behind the grazing angle of 25° (lab). Reaction products at this large angle are usually thought to arrive from osculating or "negative angle" collisions.[46] The energy spectrum is thus expected to be peaked about a Q value corresponding to fully relaxed collisions.

There are limited data available where the ejectiles have been separated by isotopes for such deep-inelastic collisions. For the ^{16}O + Ni reaction the Heidelberg group has determined[41] that
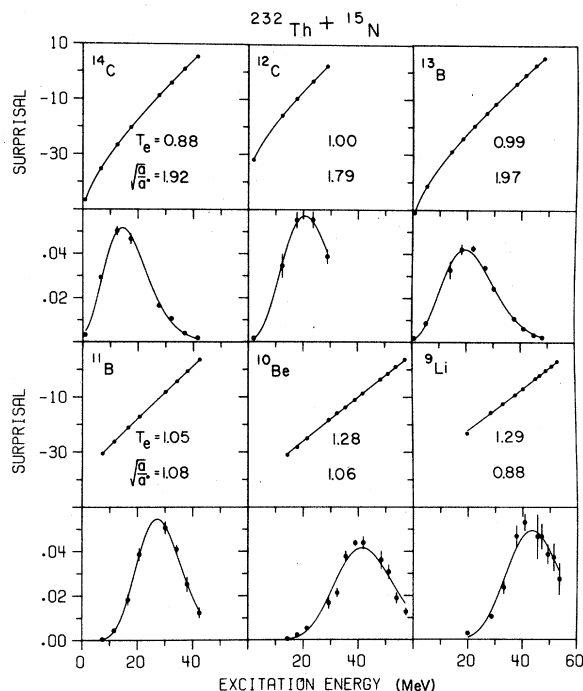

FIG. 12. Surprisal analysis for several final channels in the ^{15}N + ^{232}Th reaction (Ref. 37) at 145 MeV. Bottom scale: experimental (Ref. 37) distribution with the quoted error bars and fit. Top scale: the surprisal. Note that for several channels (such as ^{11}B and ^{10}Be) $a*$ $\simeq a$ ($\lambda_2 \simeq 0$) so that the surprisal is quite linear. (The energy scale has been corrected for the finite thickness of the target.

the dominant exit channel of mass 12 is ^{12}C. The reaction Q values for the ^{60}Ni and ^{58}Ni isotopes, comprising 94% of the natural target, differ by only 0.6 MeV, so that the measured[41] $d^2\sigma/dQd\Omega$ for the natural target can be analyzed. The results, using (3.9), are shown in Fig. 16.

The results shown in Fig. 16 provide a direct demonstration that the same constraints used to analyze the quasielastic energy spectrum also account for the strongly-damped, deep-inelastic processes. The analysis of the minor, strongly damped, component in one-or two-nucleon transfers has indeed suggested that this might be the case, but here one has a more direct test.

F. Discussion

The primary conclusion of the suprisal analysis is that the energy distributions are dominated by a single constraint—the mean value of the final excitation energy. A distribution which reproduces this mean value and is otherwise of maximal entropy accounts for most of the deviation of the actual energy spectra from the purely statistical (density of states) limit. [We use the
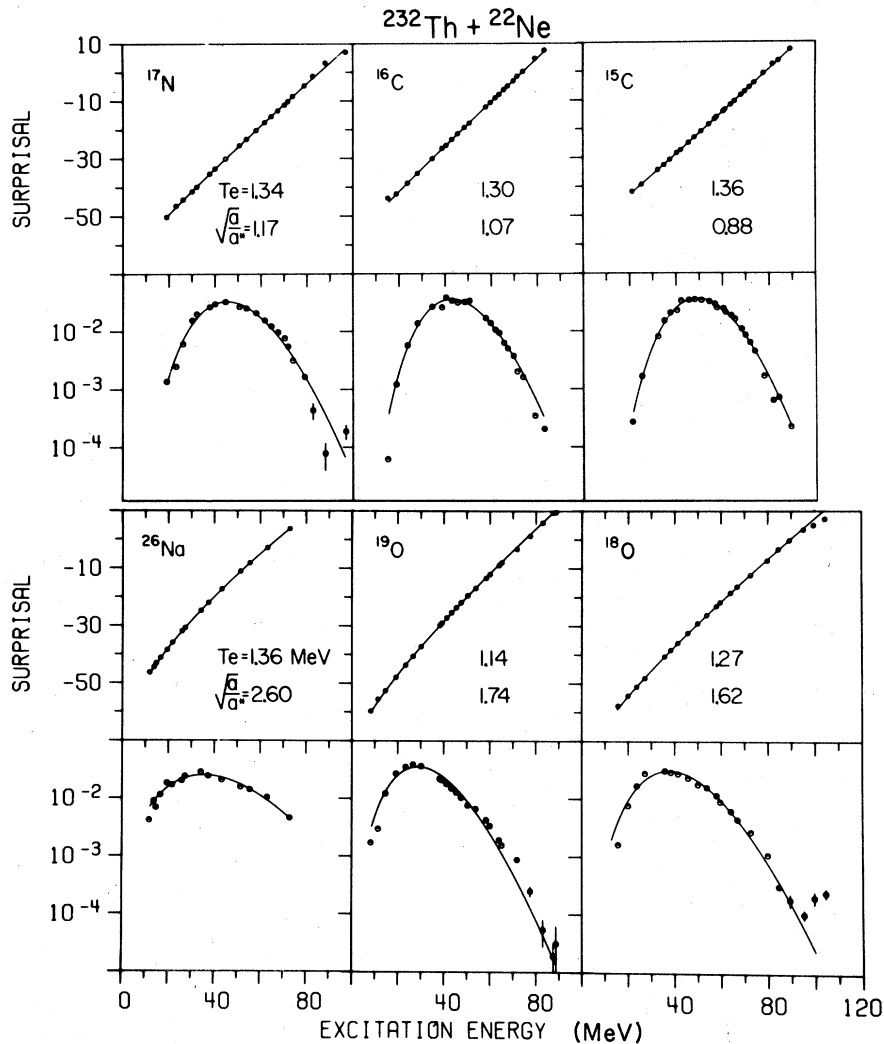
FIG. 13. Surprisal analysis of several final channels in the ^{22}Ne + ^{232}Th reaction (Ref. 38) at 174 MeV. Bottom panel: experimental distribution (with the quoted error bars). Note the quality of the fit at the low probability region which is evident in the logarithmic plot. Top panel: the surprisal using the two parameter form, Eq. (3.5). The values of the parameters T_e and $(a*/a)^{1/2}$ are given in the figure.

entropy deficiency, Eq. (2.1), as an integral measure of deviance between two distributions.] To obtain a fully quantitative fit of the measured spectra it was found necessary to introduce a second constraint, i.e., $(E*)^{1/2}$. In Sec. IV we show that the first constraint implies that the single nucleon distribution function in the ejectile is that expected at thermal equilibrium. The second constraint implies, however, that the nucleon-nucleon correlations are not fully relaxed. When the second constraint is not required (λ_2 = 0 or $a* = a$) all correlation functions have attained their thermal equilibrium value.

For such exit channels which are adjacent to the incident one (i.e., one- or two-nucleon transfers), there is an additional effect: The energy spectrum contains a smaller, second, component. By its more negative optimal Q value and by the fact that it is well described by a single constraint this component is nearly fully relaxed. It probably results from a transfer of nucleons in both directions such that the net transfer is small.

IV. MICROSCOPIC INTERPRETATION OF THE CONSTRAINTS

The presentation of the results in Sec. III was purely phenomenological. In this section we begin to explore the implications of the results. To do so it is convenient to take advantage of the thermodynamiclike character of the formalism. Hence this section provides an analysis of the in-
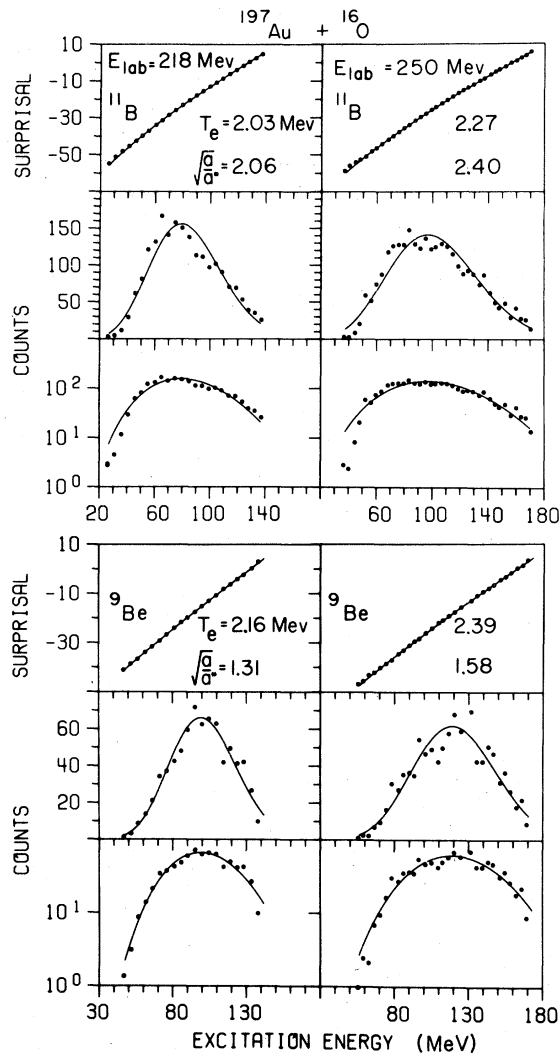
FIG. 14. Surprisal analysis of the ^{197}Au(^{16}O, ^{9}Be)^{204}Bi and the ^{197}Au(^{16}O, ^{11}B)^{202}Pb reactions (Ref. 39) at 218 and 250 MeV. The two parameter fit, Eq. (3.5), was employed. Using a weighted Q_{gg} value, excellent agreement was obtained for the (^{16}O, Li) channels where the ^{6}Li and ^{7}Li isotopes were not resolved.

FIG. 15. Surprisal analysis of the one-nucleon transfer reaction ^{197}Au(^{16}O, ^{15}N)^{198}Hg at 218 and 250 MeV. A two component fit, Eq. (3.8), was employed. The relative contribution of the strongly damped component is larger at the higher energy. Indeed, in general, the higher the incident energy above the entrance Coulomb barrier, the more significant is the contribution of the nearly relaxed component. Also, at these higher energies two- (or even three-) nucleon transfer reactions also show the presence of the relaxed component.

FIG. 16. Surprisal analysis of the energy distribution in the deep-inelastic Ni(^{16}O, ^{12}C)Zn collision at 96 MeV. A two parameter fit [Eq. (3.5)] is employed. As expected for an osculating collision, the distribution is strongly damped with $a^* > a$ (which is typical of multi-nucleon transfer channels, cf. Table II).

ternal energy distribution in the nucleus which is cast in statistical-mechanical terms. The implications of the constraints for the dynamics of the collision are discussed in Sec. V.

A. The Fermi-gas model

The experimental results refer to the fraction $P(E^*)\Delta E^*$ of heavy ejectiles with internal energies in the range E^*, $E^* + \Delta E^*$. There are very many (essentially a continuum of) quantum states of the nucleus in any such energy range. To learn something of the distribution of such states we adopt the Fermi-gas (or single-particle) model.[31]
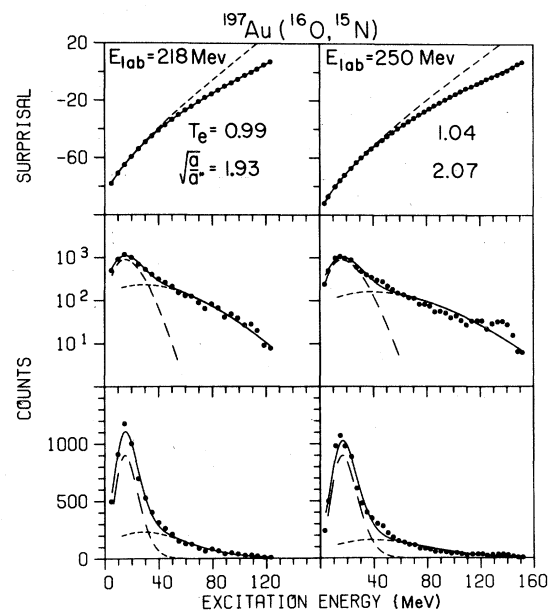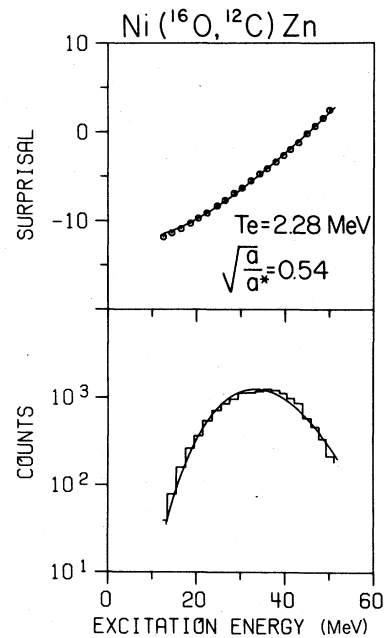
Each quantum state of the nucleus is then identified by a sequence of occupation numbers $\tilde{n}$ $= (n_1, n_2, \cdots, n_\nu \cdots)$, where n_ν $(n_\nu = 0$ or $1)$ is the population of the single-particle level ϵ_ν and $\sum n_\nu = A$. The excitation energy of the nucleus is E^*,

$$E_0 + E^* = \sum_\nu n_\nu \epsilon_\nu, \tag{4.1}$$

where E_0 is the ground state energy $(E_0 = \sum' \epsilon_\nu$, where the sum is over all levels below the Fermi energy $\epsilon_F)$.

The number of quantum states when the excitation energy is in the range E^*, $E^* + \Delta E^*$, is $\rho(E^*)\Delta E^*$, where $\rho(E^*)$ is the density of levels in the Fermi gas[31] (cf. Sec. II C). The results of Sec. III can thus be summarized: The probability of the quantum state n in the heavy residual nucleus is [cf. (2.4), (2.16), and (3.9)]

$$p_{\tilde{n}} = \exp(-\lambda_1 E^* - \lambda_2 E^{*1/2})/Z(\lambda_1, \lambda_2). \tag{4.2}$$

All the microscopic states at the same excitation energy are thus equally probable. Z ensures that $p_{\tilde{n}}$ is normalized:

$$Z = \sum_{\tilde{n}} \exp(-\lambda_1 E^{*1/2})$$
$$= \int_0^E dE^* \rho(E^*) \exp(-\lambda_1 E^* - \lambda_2 E^{*1/2}), \tag{4.3}$$

where E (the total energy, $= E_i + Q_{gg}$) is the highest possible value of E^*. In practice, λ_1 is sufficiently large to ensure that the integrand in (4.3) is negligible at $E^* = E$ so that the upper limit can be extended to infinity. By analogy to statistical mechanics Z will be termed "the partition function." For future use it is convenient to regard Z as a function of $\lambda \equiv \lambda_1$ and of $a^* = (a^{1/2} - \lambda_2/2)^2$.

It is of interest to compare the distribution (4.2) to the canonical (or thermal equilibrium) distribution in a Fermi gas:

$$p_{\tilde{n}}^c = \exp(-\beta E^*)/Z(\beta, a), \tag{4.4}$$

$$Z(\beta, a) = \int_0^\infty dE^* \rho(E^*) \exp(-\beta E^*), \tag{4.5}$$

where $p_{\tilde{n}}^c$ does factorize as a product of one-particle distribution functions [cf. (4.1)]. The presence of the second constraint implies that the actual distribution after the collision $p_{\tilde{n}}$, Eq. (4.2), does not. The excitations in the heavy residual nucleus are therefore correlated, except if $\lambda_2 = 0$. Despite this correlation we shall find it possible to show that the mean occupation numbers $\langle n_\nu \rangle$,

$$\langle n_\nu \rangle = \sum_{\tilde{n}} n_\nu p_{\tilde{n}}, \tag{4.6}$$

do have that dependence on ϵ_ν:

$$\langle n_\nu \rangle = 1/\{1 + \exp[\beta(\epsilon_\nu - \epsilon_F)]\}, \tag{4.7}$$

characteristic of a degenerate Fermi gas in thermal equilibrium.[47] It is only in the two-particle $(\langle n_\nu n_{\nu'} \rangle)$ and higher correlation functions that one discerns the presence of the second constraint. It should, however, be stressed that these conclusions do depend on the first constraint $\langle E^* \rangle$ being linear in the $\langle n_\nu \rangle$'s and on the second constraint $\langle E^{*1/2} \rangle$ not being of this type, and are not necessarily valid in general. Of course, if only the first constraint is required, then all correlation functions have the dependence expected at thermal equilibrium.

B. The mean occupation number

To compute the mean occupation number for the distribution $p_{\tilde{n}}$ it is convenient to make use of the observation that all states $\tilde{n}$ at the same energy are found to be equiprobable. Hence we can first compute $\langle n_\nu \rangle(E^*)$,

$$\langle n_\nu \rangle(E^*) = \sum_{\tilde{n}} n_\nu \delta \left(E_0 + E^* - \sum_\nu n_\nu \epsilon_\nu \right)/\rho(E^*),$$
$$\rho(E^*) = \sum_{\tilde{n}} \left(\delta \quad E_0 + E^* - \sum_\nu n_\nu \epsilon_\nu \right), \tag{4.8}$$

the mean particle number at the energy E^*, and then average it over $P(E^*)$. The first part is standard,[31] if lengthy, leading to the (approximate) result

$$\langle n_\nu \rangle(E^*) = 1/\{1 + \exp[(a/E^*)^{1/2}(\epsilon_\nu - \epsilon_F)]\}. \tag{4.9}$$

We have verified that the validity conditions on the result of (4.9) [Ref. 31, p. 284, (2B-20) and (2B-22), in particular] are satisfied for the systems of interest in the study. The second stage

$$\langle n_\nu \rangle = \int_0^E dE^* \langle n_\nu \rangle(E^*) P(E^*) \tag{4.10}$$

is readily carried out by a change of variable from E^* to $y = a^* E^*/a$. This brings the integrand to the same form as that of a Fermi gas in thermal equilibrium. By extending the upper limit to infinity one obtains the result (4.7) with

$$\beta = \lambda(a/a^*)^{1/2}. \tag{4.11}$$

As before, $\lambda \equiv \lambda_1$ and $a^* \equiv (a^{1/2} - \lambda_2/2)^2$.

C. The excitation temperature

For light sources the brightness temperature has long been defined[48] as the temperature of a blackbody with the same mean number of photons

in the same frequency range. (Different frequencies from the same source may, of course, have different brightness temperatures.) We propose to introduce a similar definition for fermions and argue that the results of the analysis of energy disposal demonstrate the utility of such a definition. For simplicity we shall measure the temperature in energy units. To convert to degrees the results need be divided by Boltzmann's constant k ($k = 8.6210^{-11}$ MeV/deg).

In a Fermi gas at equilibrium only such nucleons that are within T below the Fermi level can be thermally excited. Hence, the temperature is a measure of the number of excited nucleons. Since a measures the density of single nucleon states we can estimate the mean number of excitons in a Fermi gas at thermal equilibrium as aT. (An exciton is a hole below the Fermi level or a particle above it.) The distribution of mean exciton number at thermal equilibrium is[31]

$$\langle n_\nu^e \rangle = 1/[1 + \exp(\epsilon_\nu^e/T)], \qquad (4.12)$$

where $\epsilon_\nu^e = |\epsilon_\nu - \epsilon_F|$. Summing (4.12) over all states ν one verifies that the mean number of excitons is indeed aT. Hence we define the excitation temperature by

$$T_e = \epsilon_\nu^e / \ln(\langle n_\nu^e \rangle^{-1} - 1), \qquad (4.13)$$

where $\langle n_\nu^e \rangle$ is the mean number of excitons of energy ϵ_ν^e in the Fermi system. The definition (4.13) holds whether the system is or is not in thermal equilibrium. If it is, $T_e \equiv T$ and is independent of ϵ_ν^e.

The results on energy disposal in the heavy-ion transfer reactions analyzed in this paper can be summarized: The residual nucleus has a constant (i.e., ϵ_ν^e-independent) excitation temperature which is readily estimated [cf. (3.10) and (4.11)] by

$$T_e = (E_{mp}^*/a)^{1/2}. \qquad (4.14)$$

Such properties of the residual nucleus that depend only on the one-particle distribution function $\langle n_\nu \rangle$ can thus be computed as if the nucleus is at thermal equilibrium at the temperature T_e. As we show next this is no longer the case for such properties [e.g., the width of the distribution $P(E^*)$] which depend on the two-particle (or higher) correlation functions.

D. The variance of the energy distribution

The variance of the distribution is the simplest measure of the two-particle correlation function

$$\langle (\Delta E^*)^2 \rangle \equiv \langle (E^* - \langle E^* \rangle)^2 \rangle$$

$$= \sum_\nu \sum_{\nu'} \epsilon_\nu \epsilon_{\nu'} (\langle n_\nu n_{\nu'} \rangle - \langle n_\nu \rangle \langle n_{\nu'} \rangle). \qquad (4.15)$$

By an explicit computation of the average of $(E^* - \langle E^* \rangle)^2$ over the distribution $P(E^*)$ one readily verifies that

$$\langle (\Delta E^*)^2 \rangle = (a/a^*)^{1/2} \langle (\Delta E^*)^2 \rangle^c. \qquad (4.16)$$

Here $\langle (\Delta E^*)^2 \rangle^c$ is the variance of a canonical (i.e., thermal) distribution at the temperature T_e. If $a^* > a$ (λ_2 negative), the width of the observed distribution is narrower than the width for a nucleus at equilibrium at the temperature T_e and conversely if $a^* < a$.

An estimate of the width can be obtained from the estimate

$$\langle (\Delta E^*)^2 \rangle^c = T_e^2 \partial \langle E^* \rangle^c / \partial T_e$$

$$= 2aT_e^3 \simeq 2E_{mp}^{3/2}/a^{1/2}. \qquad (4.17)$$

Hence

$$\langle (\Delta E^*)^2 \rangle \simeq 2E_{mp}^{3/2}/a^{*1/2}. \qquad (4.18)$$

The result should be compared to the estimate (3.12) for the FWHM.

In general, using the form (3.9) one readily verifies that the nth central moment of $P^{ME}(E^*)$ is given by

$$\langle (E^* - \langle E^* \rangle)^n \rangle = (-1)^{n-1} \partial^{n-1} \langle E^* \rangle / \partial \lambda_1^{n-1} \qquad (4.19)$$

This result is easily shown to be valid irrespective of the presence of additional constraints. If we set $\beta = 1/T_e$ then, using (4.11),

$$\langle (E^* - \langle E^* \rangle)^n \rangle = (a/a^*)^{(n-1)/2} \langle (E^* - \langle E^* \rangle)^n \rangle^c. \qquad (4.20)$$

Since [cf. (4.1)] successively higher energy moments correspond to successively higher order nucleon correlation functions, the result (4.20) is the formal summary of our results. For $n = 1$, $\langle E^* \rangle = \langle E^* \rangle^c$ or the single nucleon occupation numbers are those at thermal equilibrium. For $n > 1$, the moments or the correlation functions increasingly deviate from their canonical value, except if $a^* = a$.

E. The second constraint

The second constraint was shown to govern the width of the energy distribution. This raises the question as to why it is $\langle E^{*1/2} \rangle$ rather than $\langle E^{*2} \rangle$ which is used as the second constraint. The answer provided by the independent particle model used in this section is that it is the width of the exciton (particle-hole) distribution rather than the width of the energy distribution that acts as the second constraint.

An explicit computation of the variance of the exciton distribution for a degenerate Fermi gas at a total energy E shows that (Eq. 2B-33 of Ref. 31)

$$\langle (n^e - \langle n^e \rangle)^2 \rangle (E^*) \equiv \sum_\nu \left[n_\nu^e - \langle n_\nu^e \rangle (E^*) \right]^2 \delta \left(E^* - \sum_\nu n_\nu^e \epsilon_\nu^e \right) \Big/ \rho(E^*) \simeq (aE^*)^{1/2}. \tag{4.21}$$

Upon averaging over the E^* distribution one sees that $\langle E^{*1/2} \rangle$ determines the variance of the exciton distribution.

As in the exciton model,[49] we argue that the particle-hole distribution following the collision is not fully equilibrated. Rather, it can be characterized in terms of its mean and variance. The average single nucleon occupation number is fully characterized by the mean and hence has an equilibrium dependence on the excitation energy ϵ_ν. The excitation temperature is, however, different for the different exit channels. The nucleon-nucleon correlation functions do not have an equilibrium dependence on the excitation energy. The mean and the variance of the exciton distribution suffice, however, to determine the distribution $p_{\hat{n}}$ [cf. (4.2)] of all nucleons and hence to determine all correlation functions. Further support for the choice of $E^{*1/2}$ rather than E^{*2} as the second constraint is provided by the observation that $\langle E^{*1/2} \rangle$ increases with increasing number of transferred nucleons. As in the exciton model[49] one can say that each transferred nucleon gives rise to additional particle-hole excitations in the residual nucleons and hence increases the variance of the exciton distribution.

V. SUM RULE FOR ENERGY DISPOSAL

It is clearly of interest to provide a dynamical interpretation of the constraints. Theory offers the following line of reasoning: A constraint is a reflection of a quantity which is conserved by the dynamics. If a Hamiltonian can be introduced then such quantities can, in principle, be identified and explicit examples have been worked out for simple collision problems. The theory shows[18,19] that such a conserved quantity is related to the constraints by

$$I_r(\gamma) = \sum_s G_{rs} A_s(\gamma),$$

where the coefficients G_{rs} have different values before and after the collision. Since, however, the value of $\langle I_r \rangle$ is conserved it follows that the final post-collision values of the constrained variables must be linearly dependent on their initial values.[18] Such a relation is referred to as a sum rule. A physical interpretation of the constraint is thus a model which explains the origin of the sum rule.

For multinucleon transfers the dominant constraints are the kinetic energy and normalization of the probabilities. The initial kinetic energy is well defined and $\langle 1 \rangle = 1$. Hence the sum rule is

$$\langle E_f \rangle = sE_i + \rho. \tag{5.1}$$

Here $\langle E_f \rangle$ is the mean value of the final kinetic energy in the center-of-mass system for a given arrangement channel. $\langle E_f \rangle = \langle Q \rangle + E_i$ where Q is the Q value of the reaction, and

$$\langle E^* \rangle = Q_{gg} - \langle Q \rangle = E_i + Q_{gg} - \langle E_f \rangle.$$

The coefficients s and ρ are independent of the initial kinetic energy but do depend on the arrangement channel (i.e., on the number and kind of nucleons transferred) and on the total energy. The very same sum rule has been found valid for atom transfer in molecular collisions.[17,50]

The observation that the distribution of final kinetic energy in heavy-ion transfer reactions is peaked has led to a number of models[9-15,36,40] for the most probable Q value. Their common characteristic is that if the mean rather than the most probable Q is employed they all conform to the functional form (5.1). Here we examine a simple model which with one additional approximation reduces to the Q-matching condition of Buttle and Goldfarb[9] while under another approximation reduces to the kinematic constraints of Brink[11] and of Siemens et al.[10] The model remains simple without either approximation. By introducing explicit account of tangential friction[6,13,46,51] (with a friction coefficient which is a function of the total energy but not of the exit channel), we obtain an essentially quantitative expression for $\langle E^* \rangle$.

A. Q Matching

The transfer of nucleons is assumed to take place at the distance of closest approach. In other words, up to the transfer the trajectory corresponds to (the first half of) an elastic trajectory in the incident channel. Past the transfer the system exits along an elastic trajectory in the final channel. For collisions at or about the grazing angle these elastic trajectories are dominated by Coulomb forces. Hence the distance of closest approach in the jth channel ($j = i$ or f) is

$$D_j = Z_a Z_A e^2 / E_j \xi_j. \tag{5.2}$$

E_j is the c.m. kinetic energy and $\xi_j = 2/(1 + 1/\sin\theta_j)$.

$2\theta_j$ is the deflection angle of a Rutherford trajectory at the energy E_j for ions of charges Z_a and Z_A, respectively, $\theta = \theta_i + \theta_f$.

Owing to the mass transfer, the coordinate for the relative motion is not quite the same in the incident and exit channels. If, as an additional approximation, one neglects this recoil effect (and sets $\theta_i = \theta_f$) then the orbit matching condition $D_f = D_i$ leads to the optimal Q value[9]:

$$Q_{\text{opt}} = [(Z_b Z_B - Z_a Z_A)/Z_a Z_A]E_i, \qquad (5.3)$$

or $\rho = 0$ and $s = Z_b Z_B / Z_a Z_A$, where the reaction is $a + A \to b + B$. The neglect of recoil effects is reflected in that (5.3) predicts no kinetic energy loss for a mass transfer which is not accompanied by charge transfer. The final channels which correspond to the different isotopes (same charge transfer but different mass transfers) are thus predicted to have the same optimal Q value. The experimental results, Fig. 17, indicate that mass transfer does matter. It can be allowed for by requiring matching in momentum (part B) and by introducing a recoil correction[12] (part F).

B. Momentum transfer matching

Rather than orbit matching one can consider matching in momentum.[10,11] In the reaction $a + A \to b + B$ let m nucleons be transferred from a to A and n nucleons be transferred in the opposite direction so that $a - m \equiv b - n$. At the point of closest approach the momentum is entirely in the tangential direction (since its radial component is, by definition of closest approach, zero). The momentum matching condition is

$$\vec{p}_a - \vec{p}_m = \vec{p}_b - \vec{p}_n, \qquad (5.4)$$

where $\vec{p}_m$ and $\vec{p}_n$ are the momenta of the transferred nucleons:

$$\vec{p}_m = (m/a)\vec{p}_a, \quad \vec{p}_n = (n/A)\vec{p}_A, \qquad (5.5)$$

and $\vec{p}_a$ and $\vec{p}_b$ are the momenta of a and b, i.e., the relative momenta (at the point of closest approach) before and after the transfer. The corresponding kinetic energies are

$$\epsilon_i = p_a^2/2\mu_i, \quad \epsilon_f = p_b^2/2\mu_f, \qquad (5.6)$$

where μ is the reduced mass. From (5.4) and (5.5)

$$\vec{p}_b = \left(1 - \frac{m}{a} - \frac{n}{A}\right)\vec{p}_a \qquad (5.7)$$

and

$$\epsilon_f = (\cos^2\beta)\epsilon_i, \qquad (5.8)$$

where

$$\cos^2\beta = (\mu_i/\mu_f)\left(1 - \frac{m}{a} - \frac{n}{A}\right)^2$$
$$= \left(1 - \frac{m}{a} - \frac{n}{A}\right)\left(1 - \frac{m}{B} - \frac{n}{b}\right). \qquad (5.9)$$

$\cos^2\beta$ is dimensionless and is between zero and unity. The kinetic energy loss due to the transfer is

$$\Delta\epsilon \equiv \epsilon_f - \epsilon_i = -(\sin^2\beta)\epsilon_i. \qquad (5.10)$$

For grazing collisions the kinetic energy at the distance of closest approach is

$$\epsilon_j = E_j - V_j^C(D_j), \qquad (5.11)$$

where $V^C(D)$ is the Coulomb repulsion at the separation D. Defining, as usual, Q_{eff} as the Q value corrected for Coulomb energies in the entrance and exit channels, $Q_{\text{eff}} = Q + \Delta V^C$, one has from (5.10) and (5.11) that the optimal Q_{eff} value is given by

$$Q_{\text{eff}}^{\text{opt}} = -(\sin^2\beta)[E_i - V_i^C(D_i)]. \qquad (5.12)$$

Usually the mass transfer is small compared to the mass of the heavy nuclei. m/B and n/A are thus quite small. The factor $\cos^2\beta$ [cf. (5.9)] is then

$$\cos^2\beta \simeq 1 - \frac{m}{a} - \frac{n}{b}, \qquad (5.13)$$

$$\sin^2\beta \simeq (m + n)/\mu_i. \qquad (5.14)$$

The optimal Q_{eff} value [cf, (5.12)] is thus proportional to the total number of transferred nucleons.

C. Tangential friction

The entire discussion has thus far failed to include frictional effects.[6,13,46,51] In general, one expects the frictional force to be proportional to the velocity. The energy loss estimated by multiplying the force by the effective path length will thus be also proportional to the initial velocity.[46] Hence one may expect that at higher velocities (5.11) need be replaced by[3,13,46]

$$\epsilon_i = E_i - V_i^C - A_T v_i. \qquad (5.15)$$

Here A_T is a proportionality constant and v is the velocity. After the transfer

$$\epsilon_f = E_f - V_f^C + A_T v_f. \qquad (5.16)$$

The matching condition (5.10) now reads

$$Q_{\text{eff}}^{\text{opt}} = (E_f - V_f^C) - (E_i - V_i^C)$$
$$= -(\sin^2\beta)(E_i - V_i^C)$$
$$- A_T(v_f + v_i\cos^2\beta). \qquad (5.17)$$

This simple consideration suggests that the consistently less negative values of Q_{eff} predicted by (5.12), cf. Fig. 17, may be due to the neglect of
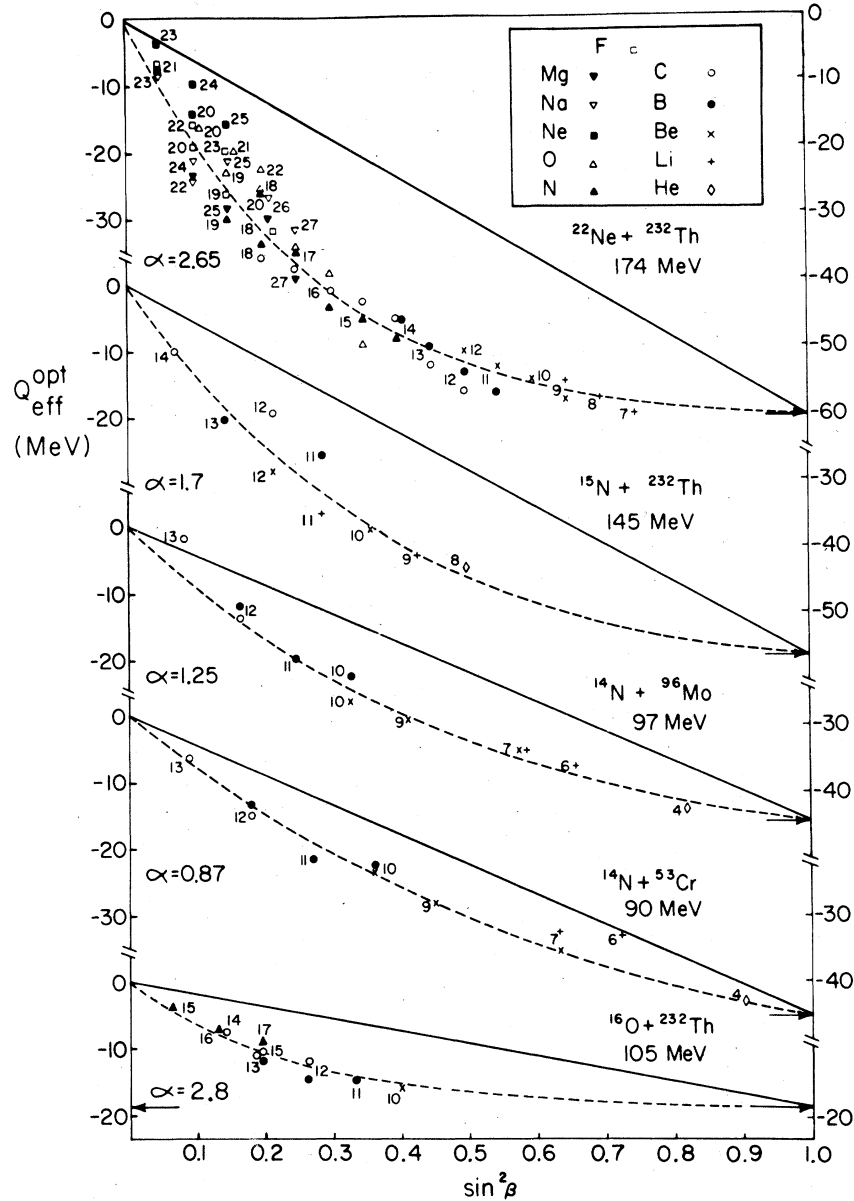
FIG. 17. $Q_{\text{opt}}^{\text{eff}}$ values (dots) vs $\sin^2\beta \simeq (n+m)/\mu_i$, where $n+m$ is the number of transferred nucleons and μ_i is the reduced mass number in the entrance channel [cf. (5.14)]. Dashed line: Eq. (5.21) which includes tangential friction with the value of α shown in the figure. The limiting $Q_{\text{eff}}^{\text{opt}}$ value for a fully relaxed collision is shown as a solid arrow. Solid line: Eq. (5.12). The sources of the experimental results (dots) and the computation of the Coulomb barrier is as in Table III. The different isotopes are identified by their A value and by their elemental names. The legend for the symbols representing the elements is given in the panel of the ^{22}Ne + ^{232}Th reaction.

friction.

While the sum rule (5.17) does represent an improvement in the right direction[3] (its second term is negative), the value of A_T is found[3] to depend on the final arrangement channel. An alternative point of view and one which requires only one friction coefficient to account for all exit chan-

nels is as follows[4,51]: For grazing collisions the rate of loss of (tangential) kinetic energy due to friction is

$$d\epsilon/dt = \mu v(dv/dt) = -\gamma v^2 = -(2\gamma/\mu)\epsilon. \qquad (5.18)$$

Over a time interval of length t the kinetic energy is thus reduced by $\exp[-(2\gamma/\mu)t]$. Assuming that

the duration of transfer is proportional to the number of nucleons transferred we have that during the osculation the fractional loss of energy due to tangential friction is [cf. (5.14)]

$$\exp[-2\gamma(t/\mu)] = \exp(-\alpha \sin^2\beta),\qquad(5.19)$$

where α is independent of the exit channel. The energy loss due to both the friction and the momentum transfer is [cf. (5.8)]

$$\epsilon_f = \epsilon_i (\cos^2\beta) \exp(-\alpha \sin^2\beta).\qquad(5.20)$$

The sum rule (5.12) now reads[52]

$$
\begin{aligned}
Q_{\text{eff}}^{\text{opt}} &\equiv \epsilon_f - \epsilon_i \\
&= -[1 - \cos^2\beta \exp(-\alpha \sin^2\beta)]\epsilon_i.
\end{aligned}\qquad(5.21)
$$

In the absence of friction ($\alpha = 0$), (5.21) reduces to (5.12).

D. Results

The comparison[52] of (5.12) and (5.21) with experimental results is shown for several reactions in Fig. 17. The results for the $^{16}O + ^{232}Th$ reaction are also given in Table III. The sum rule (5.21) does, of course, allow a single adjustable parameter (i.e., α). However, for a given entrance channel the value of α is common to all exit channels.

Previous attempts[10] to improve the agreement of (5.12) with the data have retained the linear dependence of $Q_{\text{eff}}^{\text{opt}}$ on the number $[(n+m) \propto \sin^2\beta]$ of nucleons transferred but have modified the barrier by the inclusion of an optical potential and by including a (constant) energy loss. The empirical evidence[36] is, however, quite clear: $Q_{\text{eff}}^{\text{opt}}$ is monotonically but not necessarily linearly dependent on $n+m$. Rather, the slope of $Q_{\text{eff}}^{\text{opt}}$ vs $(n+m)$ decreases as the number of transferred nucleons increases.

The functional form (5.21) provides not only a quantitative but also a qualitative account of the systematics of $Q_{\text{eff}}^{\text{opt}}$. For few-nucleon transfer ($\sin^2\beta$ low), the drop of $Q_{\text{eff}}^{\text{opt}}$ with $m+n$ is faster than that expected on the basis of momentum transfer, Eq. (5.12). [The initial slope in a plot vs $\sin^2\beta$ is $-(1+\alpha)\epsilon_i$ for (5.21) and only $-\epsilon_i$ for (5.12).] As more nucleons are transferred, $\sin^2\beta$ increases, the energy loss due to friction increases [cf. (5.19)], and the dependence on $\sin^2\beta$ becomes more moderate. Ultimately, as $\sin^2\beta \to 1$ the optimal effective Q value saturates, $Q_{\text{eff}}^{\text{opt}} \to -\epsilon_i$ or $\epsilon_f = E_f^{\text{opt}} - V_f^C \to 0$, and the final optimal kinetic energy is equal to the Coulomb barrier in the exit channel. The higher α is, the sooner (in terms of number of nucleons transferred) saturation sets in.

E. The strongly damped component

The analysis in Sec. III has indicated that the energy spectra for few-nucleon transfer processes contain a second, smaller, more nearly relaxed component. For the $^{16}O + ^{232}Th$ reaction the excellent counting statistics[21] enabled us to resolve the two components and thereby assign a reliable value to $Q_{\text{eff}}^{\text{opt}}$ of the relaxed component.

TABLE III. Energetics of the $^{16}O + ^{232}Th$ reaction at 105 MeV. [a]

Ejectile	Q_{gg} (MeV)	m	n	$\sin^2\beta$	E_f^{mp} (MeV)	V_c^f (MeV)	$\epsilon_f = E_f^{mp} - V_c^f$	$Q_{\text{eff}}^{\text{opt}}$ Experiment	Theory
^{17}N	−10.60	1	2	0.20	80.1	70.2	9.9	−8.6	−10.0
^{16}N	−10.92	1	1	0.13	82.5	70.6	11.9	−6.6	−7.3
^{15}N	−6.89	1	0	0.067	86.3	70.9	15.4	−3.1	−4.2
^{15}C	−16.09	2	1	0.20	70.1	61.5	8.6	−9.9	−10.0
^{14}C	−10.47	2	0	0.13	73.3	61.8	11.5	−7.0	−7.3
^{13}C	−13.34	3	0	0.20	69.9	62.2	7.7	−10.8	−10.0
^{12}C	−11.74	4	0	0.27	69.5	62.6	6.9	−11.6	−12.1
^{13}B	−26.90	3	0	0.20	59.3	52.4	6.9	−11.6	−10.0
^{12}B	−26.09	4	0	0.27	57.1	52.7	4.4	−14.1	−12.1
^{11}B	−22.84	5	0	0.33	57.4	53.1	4.3	−14.2	−13.5
^{10}Be	−28.07	6	0	0.40	46.2	43.2	3.0	−15.5	−14.8

[a] E_f^{mp} is the final most probable kinetic energy. The experimental value for $Q_{\text{eff}}^{\text{opt}} = \epsilon_f - \epsilon_i$, where $\epsilon_i = E_i - V_i^c = 18.45$ MeV. The theoretical value for $Q_{\text{eff}}^{\text{opt}}$ is from (5.21) using $\alpha = 2.8$.

We have suggested that the damped component is due to a process where nucleons are transferred in both directions such that, e.g., the (^{16}O, ^{13}C) and the slow component in the (^{16}O, ^{15}N) channels correspond to the same number of nucleons transferred. As a check of this interpretation we have verified that the Q_{eff}^{opt} values of the damped components are in accord with the values expected from (5.21) for the actual number of transferred nucleons, Table IV. The agreement is quite close, particularly if recoil effects (part F) are taken into account.

F. The recoil effect

When the distance of closest approach is computed as the sum of the nuclear radii

$$D_i \simeq r_0(a^{1/3} + A^{1/3}) \qquad (5.22)$$

one obtains (5.12) in the form discussed by Siemens et $al.$[10] and by Brinks.[11] A somewhat better approach is to use the actual distance of closest approach. Since only the total deflection $\theta_i + \theta_f$ is known, it is necessary to provide another relation in order to be able to determine D_i and D_f separately. [D depends on θ via ξ, cf. (5.2).] A simple relation assuming a collinear arrangement during the transfer process is

$$\delta D \equiv D_f - D_i = m\left(\frac{R_1}{a} - \frac{R_2}{B}\right) - n\left(\frac{R_1}{b} - \frac{R_2}{A}\right), \qquad (5.23)$$

where R_1 and R_2 are the radii of the two cores. The use of this relation leads to the physically realistic conclusion that $|\theta_i - \theta_f|$ increases as

more nucleons are transferred. However, the corrections to (5.12), while in the right direction do not suffice to fully account for the fact that the actual energy loss is systematically larger than that predicted by (5.12). If the recoil correction is applied to (5.21), the results are somewhat better than those shown in Fig. 17 but the correction is a small one.

G. Transport equations

We have discussed the use of models for deriving successively more accurate sum rules for the optimal final kinetic energy. Theory shows[18,19] that sum rules can be derived directly from the fundamental equations of motion. Specifically, if $\langle C_r \rangle$, $r = 1, \ldots, M$ are the M mean values required to constrain the final distribution, then during the collision these mean values satisfy a $closed$ set of coupled equations of motion [e.g., Eq. (6.16) of Ref. 18]:

$$\partial \langle C_r \rangle(t)/\partial t = -\sum_s g_{sr}\langle C_s \rangle(t). \qquad (5.24)$$

Here the coefficients matrix g is independent of the initial state and the sum rules are just the integrated form of (5.24).

The coupled equations (5.24) can, of course, be obtained also from transport equations.[7] Indeed, both early and very recent studies have tended to center attention on the transport equations for the mean values. The matrix g is then precisely the transport coefficients matrix of such theories. Hence we conclude by pointing out that a route to the final distribution is to solve the transport equations for the mean values of the constraints and to determine the distribution by the procedure of maximal entropy subject to the values of the constraints.[53]

TABLE IV. Q_{eff}^{opt} values of the quasielastic and the damped components.[a]

Reaction	Quasielastic component Q_{eff}^{opt} (MeV)		Damped component Q_{eff}^{opt} (MeV)	
	From fit	From (5.21)	From fit	From (5.21)
^{232}Th (^{16}O, ^{15}N) 105 MeV	−3.1	−4.2	−13.0	−10.0
^{53}Cr (^{14}N, ^{13}C) 90 MeV	−4.5	−7.1	−22	−19.1
^{197}Au (^{16}O, ^{15}N) 218 MeV	−12	−13	−29	−33
^{197}Au (^{16}O, ^{15}N) 250 MeV	−14	−14	−41	−43

[a]The "fit" entry is from the surprisal analysis using (3.8). The result from (5.21) is computed using the actual number of transferred nucleons.

Our conclusion (Sec. IV E) that the constraints are on the mean and the variance of the exciton distribution rather than on the mean and the variance of the energy distribution has an obvious implication for the choice of variables in the phenomenological application of transport equations to describe heavy-ion reactions. Our analysis definitely supports an exciton model rather than an energy transport point of view.

VI. CONCLUSIONS

The broad, asymmetric bell shaped, energy distributions for heavy-ion induced transfer to highly excited states can be well characterized as distributions of maximal entropy (or minimal information content) subject to a constraint on the excitation energy E^* and a constraint on $E^{*1/2}$ and using a Fermi-gas level density for the residual nucleons. The interpretation of these constraints in terms of single nucleon occupation numbers has been discussed. It is suggested that the mean single nucleon occupation numbers have relaxed to a thermal distribution with an effective temperature determined by the magnitude $\langle E^* \rangle$ of the first constraint. The nucleon-nucleon correlation functions are, however, not thermal and the magnitude of $\langle E^{*1/2} \rangle$ determines the extent of this deviance. The dynamical origin of the first constraint has been discussed in terms of sum rules. A simple model, which relates $\langle E^* \rangle$ to the energy transferred per transferred nucleon and to a tangential friction term (which is proportional to the kinetic energy at the point of closest approach) gives very good agreement with experimental results. All exit channels (at a given collision energy) can be described in terms of a single damping constant α.

There are many potential extensions of the present approach. One problem, not discussed in this paper, is the systematics of the branching ratios for formation of the different isotopes. We have also not discussed the angular distributions nor the systematics of the energy-angle disposal plots.[54] The dependence of the results (and, in particular, the excitation temperature) on the collision energy should also be examined. This will further strengthen the connection to the more dynamical point of view. The transitions to discrete final states at low excitation energies, which can be described by a distorted wave approach,[23,55] can also be analyzed from the present point of view.[45] At the other end, an analysis of the mass, charge, energy, and angle distributions for deep-inelastic collisions has barely begun. Work is in progress on several of these topics.

[1]P. E. Hodgson, *Nuclear Heavy-Ion Reactions* (Clarendon, Oxford, 1978).

[2]V. V. Volkov, Phys. Rep. <u>44</u>, 93 (1978).

[3]C. K. Gelbke, C. Olmer, M. Buenerd, D. L. Hendrie, J. Mahoney, M. C. Mermaz, and D. K. Scott, Phys. Rep. <u>42</u>, 311 (1978).

[4]D. K. Scott, Lawrence Berkeley Laboratory Report No. LBL-7727, 1978 (unpublished).

[5]W. U. Schröder and J. R. Huizenga, Annu. Rev. Nucl. Sci. <u>27</u>, 465 (1977).

[6]D. H. E. Gross and H. Kalinowski, Phys. Rep. <u>45</u>, 175 (1978).

[7]See, for example, W. Nörenberg, Phys. Lett. <u>53B</u>, 289 (1974); S. Ayik, B. Schurmann, and W. Nörenberg, Z. Phys. <u>A279</u>, 299 (1976); G. Wolschin and W. Nörenberg, *ibid.* <u>A284</u>, 209 (1978); J. S. Sventek and L. G. Moretto, Phys. Lett. <u>65B</u>, 326 (1976); R. P. Schmitt, P. Russo, R. Babinet, R. Jared, and L. G. Moretto, Nucl. Phys. <u>A279</u>, 141 (1976); H. Hofmann and F. P. Siemens, *ibid.* <u>A275</u>, 464 (1977); D. Agassi, C. M. Ko, and H. A. Weidenmüller, Ann. Phys. (N. Y.) <u>107</u>, 140 (1977); J. Barrette and P. Braun-Munzinger, Nucl. Phys.

<u>A287</u>, 195 (1977).

[8]R. A. Broglia and Aa. Winther, Phys. Rep. <u>4C</u>, 153 (1972); W. E. Frahn, Nucl. Phys. <u>A302</u>, 267 (1978) and references therein.

[9]P. J. A. Buttle and J. L. B. Goldfarb, Nucl. Phys. <u>A176</u>, 299 (1971).

[10]P. J. Siemens, J. P. Bondorf, D. H. E. Gross, and F. Dickmann, Phys. Lett. <u>36B</u>, 24 (1971).

[11]D. M. Brink, Phys. Lett. <u>40B</u>, 37 (1972).

[12]J. P. Schiffer, H. J. Körner, R. H. Siemssen, K. W. Jones, and A. Schwarzschild, Phys. Lett. <u>44B</u>, 47 (1973).

[13]J. Wilczynski, K. Siwek-Wilcynska, J. S. Larsen, J. C. Acquadro, and P. R. Christensen, Nucl. Phys. <u>A244</u>, 147 (1975).

[14]T. M. Cormier, P. Braun-Munzinger, P. M. Cormier, J. W. Harris, and L. L. Lee, Jr., Phys. Rev. C <u>16</u>, 215 (1977).

[15]W. von Oertzen, Z. Phys. <u>A279</u>, 367 (1976).

[16]R. D. Levine and R. B. Bernstein, Acct. Chem. Res. <u>7</u>, 393 (1974).

[17]R. D. Levine, Annu. Rev. Phys. Chem. <u>29</u>, 59 (1978).

[18]Y. Alhassid and R. D. Levine, preceding paper, Phys. Rev. C **20**, 1775 (1979).

[19]Y. Alhassid and R. D. Levine, Phys. Rev. A **18**, 89 (1978).

[20]R. D. Levine, S. G. Steadman, J. S. Karp, and Y. Alhassid, Phys. Rev. Lett. **41**, 1537 (1978).

[21]G. G. Batrouni, J. S. Karp, S. G. Steadman, and F. Videbaek, Nucl. Phys. (to be published).

[22]See, for example, S. Goldman, *Information Theory* (Dover, New York, 1953), p. 47. The base of the logarithm serves only to determine the units.

[23]See, for example, Ref. 11 or T. Tamura, T. Udagawa, D. H. Feng, and K. K. Kan, Phys. Lett. **66B**, 109 (1977).

[24]See the appendix of Y. Alhassid and R. D. Levine, J. Chem. Phys. **67**, 4321 (1977).

[25]See Ref. 19 and Refs. 1–10 therein.

[26]The distribution is always unique. The values of the Lagrange parameters are unique if the constraints are linearly independent. See, for example, Ref. 27.

[27]Y. Alhassid, N. Agmon, and R. D. Levine, Chem. Phys. Lett. **53**, 22 (1978); J. Comput. Phys. **30**, 250 (1979).

[28]E. T. Jaynes, Phys. Rev. **106**, 620 (1957).

[29]The minimal value of $\mathcal{L}$ can exceed zero for two reasons, one of principle and one of practice. The first is that the number (n) of constraints does not suffice to fully account for the data. In this case more constraints need be included. The second is that due to inevitable scatter in the data $\min L > 0$, even though all the constraints required to fit the "true" probabilities are present. Adding constraints will only result in fitting the noise. The stopping criterion for noisy data is discussed in Ref. 30.

[30]J. L. Kinsey and R. D. Levine, Chem. Phys. Lett. (to be published).

[31]A. Bohr and B. R. Mottelson, *Nuclear Structure* (Benjamin, New York, 1969), Vol. 1, p. 155.

[32]A. H. Wapstra and K. Box, At. Data Nucl. Data Tables **19**, 177 (1977).

[33]P. Fong, *Statistical Theory of Nuclear Fission* (Gordon and Breach, New York, 1969), p. 33–41.

[34]M. Yoshie and I. Kohno, Sci. Papers I. P. C. R. **69**, 63 (1975).

[35]I. Kohno, K. Katori, T. Mikumo, T. Motobayashi, S. Nakajima, M. Yoshie, and H. Kamitsubo, J. Phys. Soc. Jpn. **42**, 1 (1977).

[36]T. Mikumo, T. Kohno, K. Katori, T. Motobayashi, S. Nakajima, M. Yoshi, and H. Kamitsubo, Phys. Rev. C **14**, 1458 (1976).

[37]A. G. Artukh, V. V. Avdeichikov, G. F. Gridnev, V. L. Mikheev, V. V. Volkov, and J. Wilczynski, Nucl. Phys. **A168**, 321 (1971).

[38]A. G. Artukh, G. F. Gridnev, V. L. Mikheev, V. V. Volkov, and J. Wilczynski, Nucl. Phys. **A211**, 299 (1973).

[39]D. K. Scott, M. Bini, P. Doll, C. K. Gelbke, D. L. Hendrie, J. L. Laville, J. Mahoney, A. Menchaca-Rocha, M. C. Mermaz, C. Olmer, T. J. M. Symons, Y. P. Viyoghi, K. Van Bibber, H. Weiman, and P. J. Siemens, Lawrence Berkeley Laboratory Report No. LBL-7729, 1978 (unpublished); C. Olmer, M. Mermaz, M. Buenerd, C. K. Gelbke, D. L. Hendrie, J. Mahoney, D. K. Scott, M. H. Macfarlane, and S. C. Pieper, Lawrence Berkeley Laboratory Report No. LBL-6553, 1977

(unpublished); C. K. Gelbke, D. K. Scott, M. Bini, D. L. Hendrie, J. L. Laville, J. Mahoney, M. C. Mermaz, and C. Olmer, Phys. Lett. **70B**, 415 (1977). We are indebted to Dr. D. K. Scott for providing us with the original data.

[40]J. Galin, D. Guerreau, M. Lefort, J. Peter, X. Tarrago, and R. Bosile, Nucl. Phys. **A159**, 461 (1970).

[41]R. Albrecht, W. Dünnweber, G. Graw, H. Ho, S. G. Steadman, and J. P. Wrum, Phys. Rev. Lett. **34**, 1400 (1975).

[42]The possibility of bidirectional transfer has been discussed in connection with diffusion models at the higher energies, e.g., L. Moretto, J. Galin, R. Babinet, Z. Fraenkel, R. Schmitt, R. Jared, and S. G. Thompson, Nucl. Phys. **A259**, 173 (1976). This paper also discusses the quasielastic and the relaxed components of the energy distributions for collisions where the angular distributions are strongly forward peaked.

[43]U. Dinur, R. Kosloff, R. D. Levine, and M. J. Berry, Chem. Phys. Lett. **34**, 199 (1975).

[44]For the information theory approach to branching ratios see R. D. Levine and R. Kosloff, Chem. Phys. Lett. **28**, 300 (1974) and in Ref. 17.

[45]Y. Alhassid, Ph.D. thesis, Hebrew University, Jerusalem, 1978 (unpublished).

[46]J. Wilczynski, Phys. Lett. **47B**, 484 (1973).

[47]See, for example, K. Huang, *Statistical Mechanics* (Wiley, New York, 1963).

[48]M. Planck, *Theory of Heat Radiation* (Blakiston, New York, 1914). See also, for example, P. T. Landsberg, *Thermodynamics* (Interscience, New York, 1961), p. 294.

[49]J. J. Griffin, Phys. Rev. Lett. **17**, 478 (1966); Phys. Lett. **B24**, 5 (1967); M. Blann, Annu. Rev. Nuc. Sci. **25**, 123 (1975).

[50]See, for example, A. Kafri, E. Pollak, R. Kosloff, and R. D. Levine, Chem. Phys. Lett. **33**, 201 (1975); E. E. Pollak and R. D. Levine, Chem. Phys. **21**, 61 (1977).

[51]R. Beck and D. H. E. Gross, Phys. Lett. **B47**, 143 (1973); J. P. Bondorf, M. I. Sobel, and D. Sperber, Phys. Rev. C **15**, 83 (1974); D. H. E. Gross, Nucl. Phys. **A240**, 472 (1975); J. R. Huizenga, J. R. Birkelund, W. U. Schröder, K. L. Wolf, and V. E. Viola, Phys. Rev. Lett. **37**, 885 (1976).

[52]The result (5.21) fails to allow for the recoil effects (Sec. F below) as it sets $D_i = D_f$. It therefore predicts the same $Q_{\text{eff}}^{\text{opt}}$ for different channels with the same number of transferred nucleons. By using (5.23) it is possible to introduce a recoil correction. This brings about a yet superior agreement with experiment. The correction is, however, small and was not included in the results shown in Fig. 17.

[53]Indeed, one can argue in general [cf. R. D. Levine and M. Berrondo, Chem. Phys. Lett. **47**, 399 (1977)] that the distribution of maximal entropy subject to a transport equation for the first two moments is the solution of the Fokker–Planck equation.

[54]V. M. Strutinsky, Phys. Lett. **44B**, 245 (1973).

[55]See, for example, R. Da Silveira, J. Galin, and C. Ngô, Nucl. Phys. **A159**, 481 (1970); N. Anyas-Weiss, J. C. Cornell, P. S. Fisher, P. N. Hudson, A. Menchaca-Rocha, D. J. Millener, A. D. Panagiotou, D. K. Scott, D. Strottman, D. M. Brink, B. Buck, P. J. Ellis, and T. Engeland, Phys. Rep. **3**, 201 (1974).